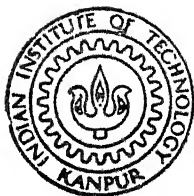# PLASTIC BEHAVIOUR OF CuAl₂

by

TAPAS CHANDA

DEPARTMENT OF METALLURGICAL ENGINEERING

INDIAN INSTITUTE OF TECHNOLOGY, KANPUR

MARCH, 1989

PLASTIC BEHAVIOUR OF CuAl₂

A Thesis Submitted
In Partial Fulfilment of the Requirements
for the Degree of
MASTER OF TECHNOLOGY

by

TAPAS CHANDA

to the

DEPARTMENT OF METALLURGICAL ENGINEERING

INDIAN INSTITUTE OF TECHNOLOGY, KANPUR

MARCH, 1989

ME - 1989 - M - CHA - 图 PLA

CERTIFICATE

This is to certify that the present investigation 'Plastic Behaviour of $CuAl_2$' has been carried out by Mr. Tapas Chanda under my supervision and that it has not been submitted elsewhere for a degree.

(G.S.MURTY)
Professor
Department of Metallurgical Engineering,
Indian Institute of Technology,Kanpur-16
U.P.,INDIA.

ACKNOWLEDGEMENT

C O N T E N T S

:::::::

LIST OF FIGURES

List of Figures Contd...

List of Figures Contd...

- -

Figure No.	Particulars	Page No

- -

- -

LIST OF SYMBOLS

T_m = Melting point in °K

σ = True stress

ε = True plastic strain

$\dot{\varepsilon}$ = Strain rate

$\dot{\varepsilon}_0'$ = Constant

n = stress exponent

m = strain rate senstivity

H = activation energy for plastic flow

V = Activation volume

b = Burgers vector

R = Gas constant

k = Boltzman constant

K = Material constant

G = Shear modulus

U = Microns

d = grain size

ρ = Dislocation density

σ_μ = A thermal component of flow stress

σ^* = Thermal component of flow stress

N = Number of activated sites per unit volume

A = Area swept out per successful fluctuations

$\dot{\gamma}_D$ = Debye frequency

L = Length of dislocation involved in activation

G^l = Total free energy

S = Entropy

d^* = Barrier width, H_0 = total enthalpy

P_1, P_2 = Load, V_1, V_2 = cross head speed

Q = Deformation activation energy
F^* = Force on dislocation.

CHAPTER - I

INTRODUCTION

1.1 GENERAL

The great impetus for the study of intermetallics has been primarily to advance fundamental behaviour of alloy systems. For many years there has been the hope that long range ordered (LRO) alloys as a group may be industrially useful. In fact they are being used in many applications which do not require high tensile strength or resistance to fracture[1] e.g. Nb_3Sn as superconducting compound, Ni_3Fe as high magnetic permeability alloy, $AuAl_2$ as thin film integrated circuit conductors, Mg_3Bi_2 as liquid semiconductors, $LaNi_5$ as hydrogen absorber, NiTi as shape memory effect alloy, LiAl & Li_5Si as battery electrodes and others.

Intermetallics[2] generally come under the category of intermediate phases which occur in the intermediate composition regions of the equilibrium diagram. The intermediate phases are broadly divided into three major groups viz. (a) Electro-chemical compounds, (b) Size-factor compounds (c) Electron compounds. The term 'compound' still persists even though many of the phases do not obey valency laws of chemistry and often exist over a wide range of composition. Electrochemical compounds have common features to that of salt like compounds since their compositions satisfy the valency laws e.g. Mg_2(Pb, Sn, Ge or Si) like CaF_2. Contrary to the behaviours of salt like compound which exhibit low conductivity, the compound Mg_2Pb shows the normal conductivity whereas in Mg_2Sn a short energy gap exists resulting it to behave like a semiconductor compound.

Size factor compounds form when the atomic diameters of the elements differ appreciably. They are of two types namely interstitial and substitutional.

When radius of the interstitial atom is higher than 0.41 and less than 0.51 to that of metal atoms, then interstitial compounds with simple crystal structure form e.g. Hydrides, Borides, Carbides etc. When it is more than 0.59 then distortion becomes appreciable and it results in a much more complicated crystal structure.

For intermediate size difference i.e. 20 to 30% $\left[\dfrac{r_{\text{large atom}}}{r_{\text{small atom}}} = 1.2\right]$ an efficient packing is achieved and they are termed as Lave's Phase. They are isomorphous with the compounds $MgCu_2$ (cubic), $MgNi_2$ (Hexagonal) or $MgZn_2$ (Hexagonal). The table (1) lists some compounds which exist in a Laves phase structure.

Table (1) <u>Compounds which exist in a Laves Phase Structure</u>

$MgCu_2$ type	$MgNi_2$ type	$MgZn_2$ type	
$AgBe_2$	$BaMg_2$	$NbCO_2$	with excess 'B' metal
$BiAu_2$	$Nb(Mn \text{ or } Fe)_2$	$TaCO_2$	
$NbCO_2$	$TaMn_2$	$TiCO_2$	
$TaCO_2$	$Ti(Mn \text{ or } Fe)_2$	$ZrFe_2$	
$Ti(Be, CO, \text{ or } Cr)_2$	UNi_2		
$U(Al, CO, Fe \text{ or } Mn)_2$	$Zr(Cr, Ir, Mn, Re)$		
$Zr(CO, Fe \text{ or } W)_2$	$Ru, Os \text{ or } V)_2$		

Hume-Rothery et al[3] have pointed out that with a particular electron to atom ratio (e/a) a particular structure will be formed and this is illustrated in Table (2).

Table(2). Some Structurally Analogous Phases

e/a = 3/2			e/a = $\frac{21}{13}$	e/a = $\frac{7}{4}$
β-Brass (B.C.C)	β-Manganese (complex cubic)	(C,P.h)	γ Brass (complex cubic)	ε - Brass (C.P.h)
(Cu; Ag or Au)Zr			(Cu,Ag or Au)	(Cu,Ag or Au)
CuBe		AgZn	$(Zn \text{ or } Cd)_8$	$(Zn \text{ or } Cd)_3$
(Ag or Au)Mg	$(Ag \text{ or } Au)_3Al$	AgCd	Cu_9Al_4	Cu_3Sn
(Ag or Au)Cd	Cu_5Si	Ag_3Al	$Cu_{31}Sn_8$	Cu_3Si
$(Cu \text{ or } Ag)_3Al$	$COZn_3$	Au_5Au	(Fe,CO,Ni,Pd	$Ag_5 Al_3$
$(Cu_5Sn \text{ or } Si)$			or Pt$)_5 Zn_{21}$	
(Fe,CO or Ni)Al				

Barrett and Massalski[4] have shown how the different factors influence to form various crystal families of alloy phases through the Fig.(1).

The intermetallics could be long range ordered or short range ordered depending on the arrangement of unlike atoms.
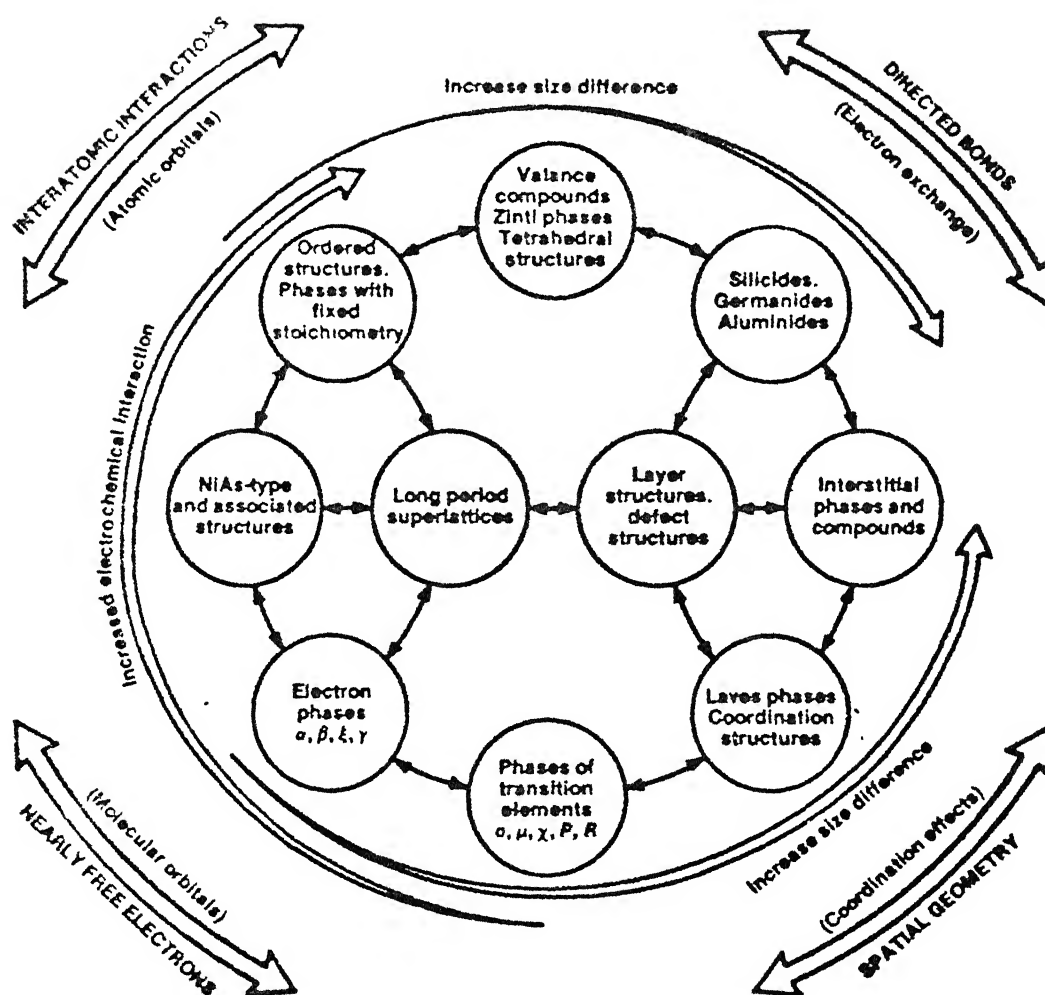
Fig. 1.   Influence of the interaction of different stabilization factors to create various crystal families of alloy phases.

Long range order is signified by the Bragg-William parameter $S = \frac{P-r}{1-r}$

where

P = the probability that an A atom site is occupied by an A atom.

r = fraction of total sites n which are occupied by A atoms. S actually varies from 0 to 1

Short range order is signified by , the Bethe's nearest neighbour parameter,

$$\sigma = \frac{q - q_r}{q_m - q_r}$$

q = no. of AB pairs

q_r = average no. of AB pairs

q_m = maximum no. of AB pairs

The relationship between S and σ is (1) $\sigma = 1$ only if S = 1 (ii) $\sigma \gg S^2$

Some commonly observed ordered structures are CuZn ($L2_0$): B.C.C. with CsCl type of structure. Other examples are Ag(Mg, Zn or Cd), AuNi, NiAl, FeAl, FeCO etc.

$AuCu_3 (L1_2)$, F.C.C. structure with copper atoms at the centres of the faces and gold atoms at the corners. Other examples are $PtCu_3$, (Fe or Mn)Ni_3, (MnFe)Ni_3, Ni_3Al, Pt_3Al.

$AuCu (L1_0)$: It is also based on F.C.C. but alternate layers (001) are made up of Cu and Au respectively. Because of the size difference the lattice is distorted into tetragonal structure having an axial ratio c/a = 0.93.

Fe_3Al (DO_3) : It is based on B.C.C. lattice but eight simple cells are necessary to describe the complete arrangement. In this structure each atom is surrounded by maximum no. of unlike atoms.

Mg_3Cd (DO_{19}) : This is based on the C.P.h lattice. Other examples are $MgCd_3$ and Ni_3Sn.

The intermetallics in general have very good phase stability, corrosion resistance, high strength both at low and high temperature and at the same time they are extremely brittle in single as well as in polycrystalline forms although exceptions are there e.g. $NiAl$, Ni_3Al (Single crystal forms). The brittleness has been explained by considering several pertinent facts[5]. limited number of slip systems or insufficient deformation mode, restricted cross slip, high Peierls Stress, a large slip vector[6] and difficulty of slip transmittal across grain boundary[7].

In order for all grains of a polycrystalline material to undergo an arbitrary change of shape at constant volume, five independent slip systems must be operative in each grain[8]. In this manner the six independent components of strain tensor for isotropic material can be provided. If this condition is not satisfied then separation of the crystals at their interfaces or fracture within the crystal is inevitable, because there are certain directions in the crystal whichcan't be extended or

compressed. A slip system is called independent if its
operation produces a change of shape that can't be produced
by a combination of slip in other systems. Among intermetallic
compound NiAl is the best documented example (9). NiAl deforms
by $\{110\}\langle 001\rangle$. So it has only three independent slip systems.
But above 400°C NiAl is ductile because some other slip systems
get activated or dislocation climb relieve the stress concen-
tration at grain boundaries. Another important feature of this
alloy (10) is that below a critical grain size ($<20\mu m$)more than
40% tensile elongation has been obtained. Slip systems of some
intermetallics is enlisted in the following table[5].

Table (3) : Some slected compounds crystal
structure and slip systems

Compound	Structure	Slip system	Reference
Ag$_2$Al	Hexagonal	$(0001)\langle 11\bar{2}0\rangle$ $(10\bar{1}0)\langle 11\bar{2}0\rangle$	Mote-et al(61)
CuGe	Hexagonal	$(0001)\langle 11\bar{2}0\rangle$ $(10\bar{1}0)\langle 11\bar{2}0\rangle$	Thomton (63)
AuCd	β'orthorhombic	$(110)[001]$	Birnabaum & Class(5
InSb	Zinc blende	$(111)[110]$ 200-500°C and (110) 25°C	Abraham et al (69)
MgCu$_2$	Laves'	$(111)\langle 110\rangle$	-Lowrie (32)
CuAuI	Tetragonal	$(111)\langle 110\rangle$	SyutKina & et al(67
PbTe	NaCl	$(110)[001]$	Rachinger (56)

Table (3) Contd.

- -

Compound	Structure	Slip system	Reference

- -

Compound	Structure	Slip system	Reference
NiAl -196 to 1000°C	Single crystal	$\{110\}\langle 001\rangle$	Ball & Small man(6
25 to 800°C	-do-	$\{100\}\langle 001\rangle$	Wasilewski,Pascoe(
-196 to 800°C	-do-	$\{213\}\langle 111\rangle$ & $\{112\}\langle 111\rangle$	Pascoe (66)
AgMg 25 - 200°C	-do-	$\{112\}\langle 111\rangle$	Kurfman (66)
25°C	Polycrystal	$\{123\}\langle 111\rangle$	Rachinger & Lottrel (56)
FeCO-V -130 - 375°C	-do-	$\{123\}\langle 111\rangle$	Jordon & Stoloff (67)
-181 to 25°C	-do-	$\{211\}\langle 111\rangle$	-do-
CuZn(25°C)	-do-	$\{110\}\langle 111\rangle$	Rachinger & Cottrel
(25°C)	-do-	$\{110\}\langle 100\rangle$ and $\{001\}\langle 100\rangle$	(56) Head et al (67)
AuCd (25°C)	-do-	$\{110\}\langle 001\rangle$	Rachinger & cottre (56)
MgTl (25°C)	-do-	$\{110\}\langle 001\rangle$	-do-
AuZn	-do-	$\{hk0\}\langle 001\rangle$ and $\{112\}\langle 111\rangle$	Schulson (67)
-196 to 200°C	Single crystal	$\{110\}\langle 001\rangle$	Rachinger and Cottrel (56)
(25°C)	Poly crystal		

- -

The second important factor i.e. restricted cross slip

plays a dominant role in some intermetallics. For example in B.C.C.

superlattice alloy FeCO-V which deforms by slip along $\langle 111 \rangle$, so there are five independent slip systems. Yet it is brittle because of the inhibition of cross slip by order thought to be the actual mechanism (Kelly & Groves- 63) for embrittlement. Other interme-tallics are Ti Al[11] and Fe-Si[12].

The third important factor is the Peierls Stress. It has been found that because of the strong directional nature of bonding in many intermetallics, the overcoming of Peierl stress is thought to be the rate controlling mechanism. Although there is no straight forward way to determine it unambiguously to be the rate controlling. Nevertheless by the process of elimination this mechanism has been ascribed to many intermetallics $MgZn_2$[13] NiAl, Fe and Alloys, Ta and alloys, Cu_3Au[14], $CuAl_2$[15].

The fourth important factor i.e. a large slip vector plays a key role in the work hardening and brittleness of ordered alloys (6).

The fifth factor i.e. transmittal of slip across grain boundaries is another important factor to which several meta-llurgists paid their attention. Westbrook & Wood (16) found that the hardness of grain boundary is greater than the bulk of the grain. They explained this in terms of excess O_2 and N_2 absorption at the G.Bs. But they failed to explain precisely why the G.B's are very resistant to spreading of plastic deformation But later work (17, 18, 19) suggests that the Ky-value (Hallpetch-

constant) is pretty high and the K_y value increases with decreasing temperature. So the deformation leads to the stress concentration at the g.b's and it is relieved through opening of a micro-crack which then propagates catastrophically. The bigger the grain size the higher will be the amount of stress concentration. In fact by decreasing grain size below 20 μm, extensive ductility in NiAl[18] has been achieved.

The birttleness of the intermetallics has been overcome by various techniques (20). They are micro/macro alloying,microstructural control, fiber strengthening and toughening.

Some intermetallics which have become commercially important from the structural point of view are TiAl, Ti_3Al, Ni_3Al, (Fe,CO, Ni)$_3$V. Zr_3Al and B_2 alluminides NiAl, FeAl and COAl. The oldest and most advanced development has taken place on Ti_3Al (Hexagonal DO_{19} structure) and TiAl (Tetragonal Li_0 structure) from the usefulness point of view. They can be prepared by casting from the melt as well as by P/m technique. Some of them can be hot rolled and forged because of their superplastic behaviour. In fact they are now being tested under service conditions in the form of turbine blades and other gas turbine components (21). One of the most outstanding intermetallics is Zr_3Al (Li_2) which has excellent irradiation resistance and has been considered for applications in the core of nuclear power reactors. It has very good combination of strength, corrosion resistance and ductility even at room temperature (22). Matérials on the basis of Ti alluminides are advantageous because of their low

densities which lead to high specific strengths. Another
advantage of this and other intermetallics e.g. Cu_3Au, Ni_3Al,
Ni_3Ge, Fe_3Ge, $(Ni, Fe)_3 Ge(L1_2)$, NiAl, FeAl, COAl, CuZn, FeCo -2V
(B_2), $TiAl(L1_0)$, Fe_3Al (DO_3), $Mg_3Cd(DO_{19})$, Ni_3V (DO_{22}), Fe,B(C16)
is that they show an anamolous temperature dependence of the flow
stress. Their flow stress increases upto certain temperature and
then decreases. The explanations which are given are many (that
too only for $L1_2$ type) but the well accepted one is due to Kear
and Wilsdorf.

The anamoly results from the anisotropy of the energy
and mobility of superlattice screw dislocations which govern
the plastic deformation in $L1_2$ type intermetallics. The screw
dislocations can split on $\{111\}$ and $\{010\}$ planes. The splitting
on $\{010\}$ is favoured energetically because the energy of the
anti-phase-boundaries (A.P.B.) between the partials is lower
on $\{010\}$ (23). However, this superlattice dislocation is sessile
because the core spreads outside the plane of A.P.B. On the
other hand the superlattice dislocation on $\{111\}$ with higher
energy is glissle because the core spreading is confined to the
slip plane (24). This glissile state is metastable since the
partials first must be co-alesced into a single dislocation
before cross slip to $\{010\}$ can occur. Hence dislocations are pri-
marily generated in $\{111\}$ plane on loading and slip is confined
to $\{111\}$ at low temperatures.With increasing temperature cross
slip to $\{010\}$ becomes possible by thermal activation by which

the dislocations are immobilised. Only at much higher tempera-
tures, the dislocations are mobilised by enhanced thermal activation
which leads to softening.

The ductility is extremely limited in most intermetallics
but it has been over come by micro and macro alloying technique.
One of the most glaring examples is the addition of 'B' ($\sim$500
ppm by wt) to Ni_3Al. This has increased the elongation from 0%
to over 50%[25] whereas macro-alloying technique has been
successful on CO_3V. Actually CO_3V brittle, hexagonal DO_{19} structure
is changed to cubic Ll_2 structure $(Fe, CO)_3V$, this in turn having
higher symmetry leads to more than 40% elongation at room tempera-
ture [26]. Also this technique has been adopted for promoting
extra slip systems in some intermetallics e.g. NiAl, Ti_3Al etc.

The intermetallics do have very good creep strength. Creep
strength is increased further by macro alloying i.e. (NiAl is
alloyed by Ti to form Ni_2Al Ti and Ni Al as second phase) that
gives creep strength equivalent to that of commerically available
superalloys MAR-M200. It's use is restricted to below 1000°C.
But $MoSi_2$ has the most outstanding creep strength and higher
than Ni_2Al Ti and it can be used above 1100°C. In fact $MoSi_2$ is
being used as electric heating elements (27) for temperatures
upto 1800°C.

1.2 $\underline{CuAl_2}$

The prime interest of studying the deformation behaviour of $CuAl_2$ is that this phase is used for reinforcement in $Al-CuAl_2$ eutectic alloy. The $Al-CuAl_2$ alloy is considered as a model system for the study of lamellar composite alloys. Ignat and Durand (28) studied the secondary creep behaviour in the temperature range of 250°C to 350°C and stresses within 30 MPa to 8 MPa. They observed two different creep behaviours both obey Dorn type of relation $\dot{\varepsilon} = A.\sigma^n \exp(^{-Q}/RT)$. Below 300°C the stress exponent (n) is 6 and Q equals to 93 KJ/mole. Over 300°C stress exponent (n) is 7.2 and Q equals to 220KJ/mole. They concluded that below 300°C deformation in the Al lamellae is the rate controlling whereas above 300°C, the deformation in the $CuAl_2$ lamellae is the rate controlling.

So by studying the deformation behaviour of $CuAl_2$, rationalisation of the behaviour of composite can be done and also the knowledge of deformation mechanism in complex-crystal structures can be extended. Moreover, $CuAl_2$ is an ordered compound which maintains its order upto the melting point. It is one of the 40 other C16 compounds which has all the requisite properties. It may possibily be used directly as a structural material. Although the melting point is low but the idea or methodology can be applied to other C16 compounds (which have very high melting point) in particular and intermetallics of other groups in general.

1.2.1   Crystal Structure & Other Details

Gniewek and Wasik[29] first studied the nature of bonding through the measurement of resistivity and Hall-coefficient. The resistivity and Hall constants values are 6.5 $\mu\Omega$ cm, + 6.9 x 10^{-5} cm^3/c respectively. They concluded (by drawing analogy with other known intermetallics) that positive Hall-constant signifies semiconductive property. Later on Zogg(30) measured the Knoop's hardness on single crystal faces in various direction and he observed the strong directional nature of bonding in $CuAl_2$. The reported value of heat of formation is $-\Delta H_f = 3.2$ KCal.[41]

The $CuAl_2$ is a C16 compact Laves phase with $\frac{R_A}{R_B} =$ 1.120, the structure is body centered tetrogonal with c/a = 0.8035. In other C16 compounds c/a varies from .74 to .89 which in turn depends on electron concentration (31). The reported values a and c are 6.04Å and 4.86Å respectively(32). The unit cell contains 4 moles AB_2. The space group is I^4/m_cm, D_{4h}^{18} (no.140). The atom positions are given by, origin at center (4/m).

Equivalent positions (0.0.0; $\frac{1}{2},\frac{1}{2},\frac{1}{2}$) +

Cu : 4   a   42   0.0, 1/4; 0.0, $\frac{3}{4}$;

Al: 8   h   mm   x,$\frac{1}{2}$+x, 0; $\bar{x}$,$\frac{1}{2}$-x, 0; $\frac{1}{2}$+x, $\bar{x}$.0;, $\frac{1}{2}$-x,x,0

- -

Co-ordination Atom	Neighbour	C.N.	Distance
Cu { Cu	2		$C/2$
Al	8		$a^2\left[(\tfrac{1}{2}-x)^2+a^2x^2+\tfrac{C^2}{16})\right]^{1/2}$
Al	Cu	4	$4\left[a^2(\tfrac{1}{2}-x)^2+a^2x^2+\tfrac{C^2}{16}\right]^{\frac{1}{2}}$
	Al	1	$d_1 = 2x\,a.2^{\frac{1}{2}}$
	Al	2	$d_2 = \left[2(\tfrac{1}{2}-2x)^2 a^2+\tfrac{C^2}{4}\right]^{\frac{1}{2}}$
	Al	4	$d_3 = \left[4x^2a^2+\tfrac{C^2}{4}\right]^{\frac{1}{2}}$
	Al	4	$d_4 = \left[\tfrac{a^2}{4}+a^2(\tfrac{1}{2}-2x)^2\right]^{\frac{1}{2}}$

- -

In other C16 compounds x varies from 0.15 to 0.175.
The isometric view has been given in fig. (2a). Each Cu atom
is surrounded by 8Al atoms and it has, in addition 2 Cu atoms
as a neighbour at a distance of $C/2 = 2.43\overset{\circ}{A}$.

Each Al atom has 4 Cu atoms as nearest neighbours and
it is surrounded by a total of 11 (1+2+4+4). Other Al atoms at
a distance d_1, d_2, d_3, d_4 (32) respectively. The structure is
better described Hägg (33) as Al atoms form two sets of mutual
orthogonal planes with a dense packing of hexagons (honey comb
structure), parallel to (110) and (1$\bar{1}$0) respectively and the
hexagons of the different sets are fully interlocking. The
Cu atoms are situated in the channels parallel to C-axis, which

are formed by this interlocking honey comb structure.
The (001) and (110) projections of the idealised $C16$
type structure is given in the Fig.(2b).

The $CuAl_2$ phase is of variable compositions[34].
This phase crystallizes directly from the melt (some authors
claim that it forms peritectically [35]. The $CuAl_2$ has
unique structural properties which have not been observed in
other C16 compounds. The stability range of $CuAl_2$ lies outside
the exact stoichiometric composition : $CuAl_2$ is slightly defi-
cient in Cu at all temperatures. The homogeneity at 548°C
extends from 67 at % (46.4 wt %) to 68.05 at % (47.5 wt %)
Al and at 400°C from 66.8 at % (46.1 wt %) to 67.35 at % (46.7
wt %) Al. The ideal composition of $CuAl_2$ 66.67 at % (45.9 wt %)
Al lies outside the homogeneity region. About the type of defects
(30) there is a lot of disagreement among several authors. The
phase diagram (34) is reproduced in Fig. (3).

The only paper which dealt with the solid solubility
of $Cu Al_2$ is due to Karou et al (36). They found by experiments
(E.D.X-Ray spectrometry - X-Ray diffraction etc.) that Be of
the order of 0.8 - 2.07 wt % could be dissolved in $Cu Al_2$. For
.8 wt % Be the stochiometric composition would become $CuAl_{1.9}$
$Be_{0.1}$.
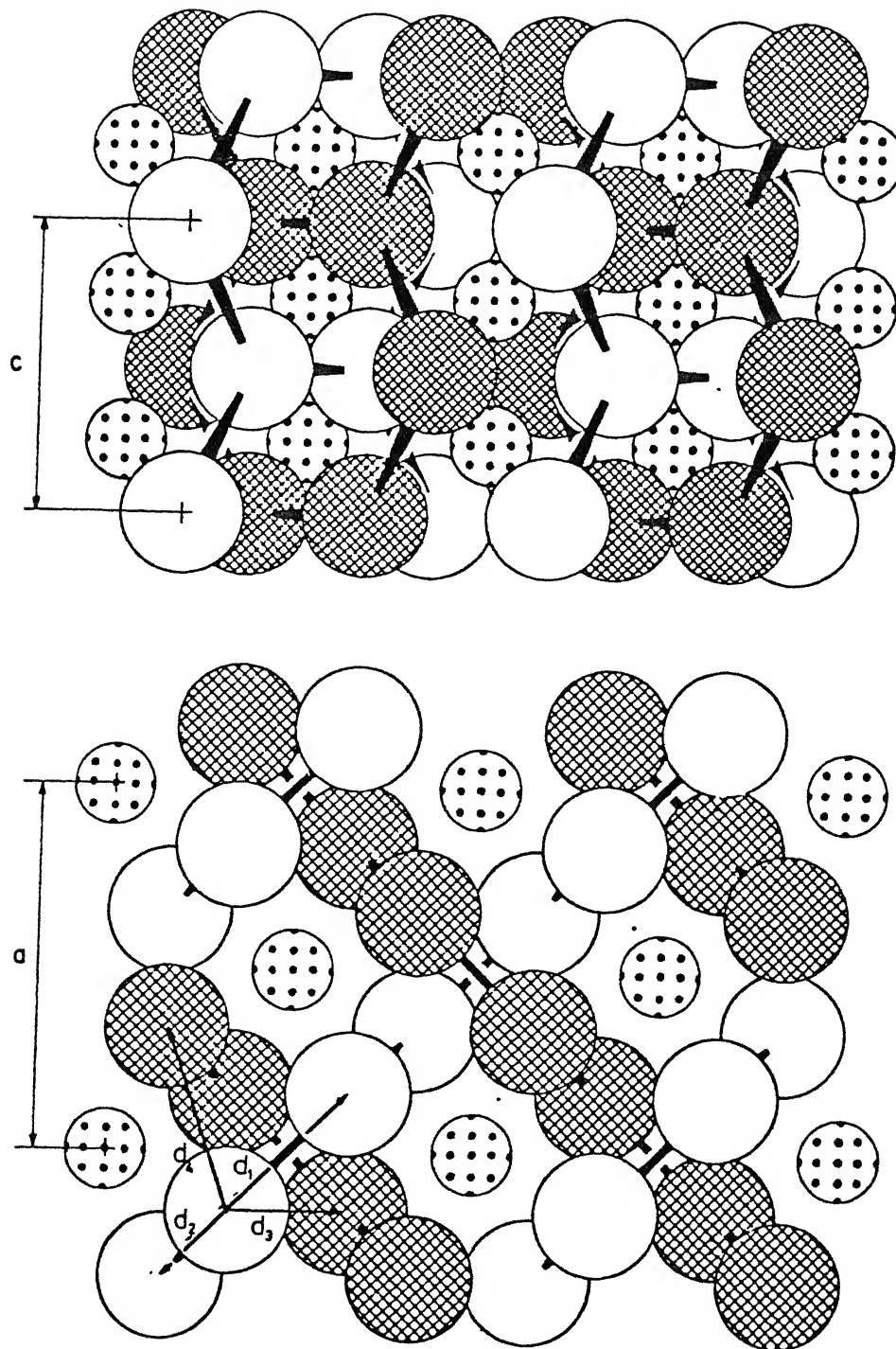
Fig. 2(b). The (001) and (110) projections of the idealized C16-type structure AB_2. The B-atoms lying in the (110) hexagon network are shaded to distinguish them from B-atoms in the $(1\bar{1}0)$ hexagon network. A-atoms have been given a smaller diameter.
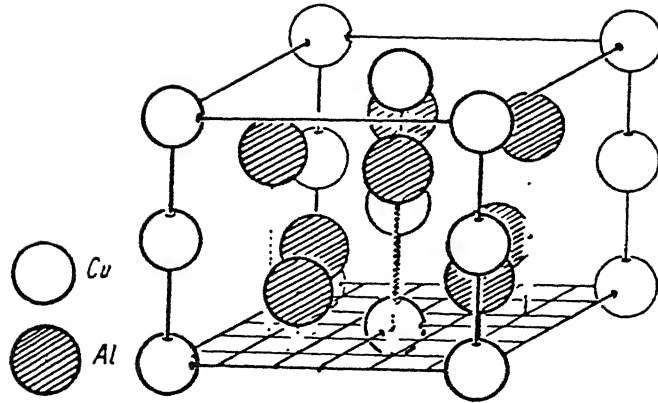
Fig. 2(a). Isometric view of CuAl₂ (C16) crystal structure.
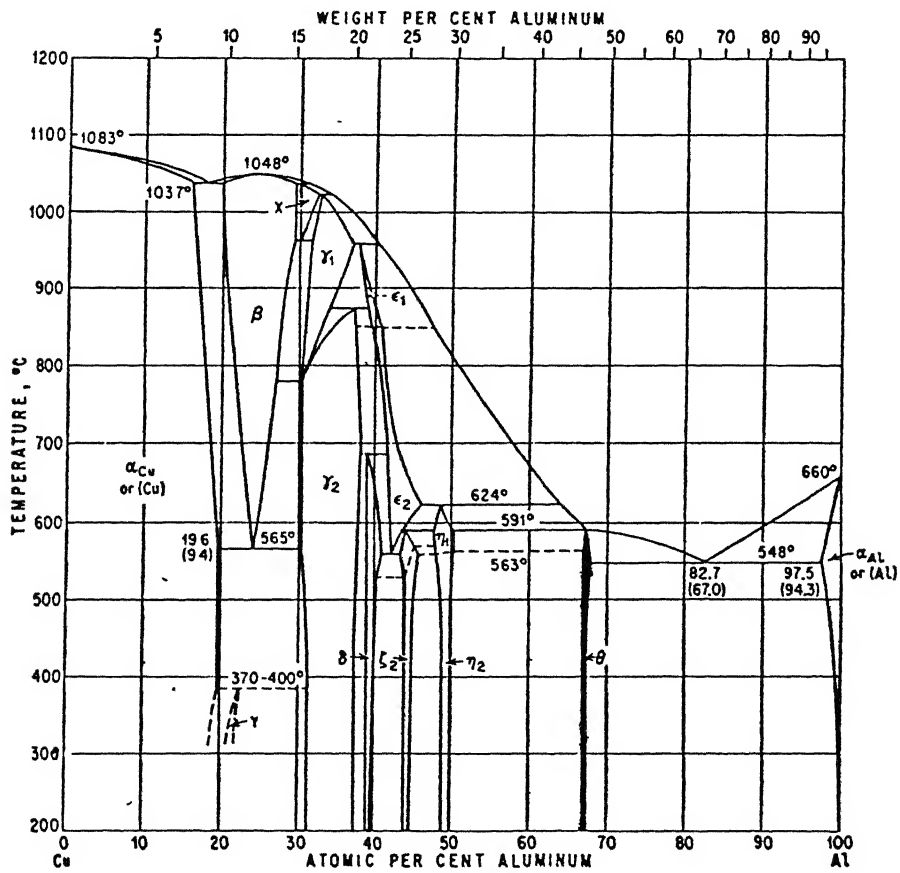
Fig. 3. Phase diagram of Cu-Al alloy system[34].

1.2.2 DEFORMATION BEHAVIOUR

(a) Elastic behaviour: This behaviour was studied by Pribourg-Blane et al through the measurement of elastic constants by Ultrasonic velocity technique and extensometric technique on single crystal of known orientation. Both the values are quite near to each other. Because of the higher reliability in U.V. technique only those values have been reproduced (37)

$$C_{11} = (159 + 0.3) \times 10^{10} Pa \qquad S_{11} = (780 \pm 8) \times 10^{-14} Pa^{-1}$$

$$C_{33} = (16.3 \pm 0.25) \times 10^{10} Pa \qquad S_{33} = (707 \pm 6) \times 10^{14} Pa^{-1}$$

$$C_{13} = (5.0 \pm 0.25) \times 10^{10} Pa \qquad S_{13} = (-156 \pm 0.4) \times 10^{-14} Pa^{-1}$$

$$C_{12} = (6.3 \pm 0.25) \times 10^{10} Pa \qquad S_{12} = (-261 \pm 0.9) \times 10^{-14} Pa^{-1}$$

$$C_{44} = (2.90 \pm 0.02) \times 10^{10} Pa \qquad S_{44} = (3450 \pm 20) \times 10^{-14} Pa^{-1}$$

$$C_{66} = (4.60 + 0.01) \times 10^{10} Pa \qquad S_{66} = (2174 \pm 2) \times 10^{-14} Pa^{-1}$$

They also calculated the Young's Modulus, poisson's ratio and they are $10.6 \times 10^{10} Pa$ and 0.31 respectively.

This value agreed well with the reported value of $(9.83 \times 10^{10} Pa)$ Cabarat et al (38) on polycrystalline specimen.

are reproduced in Fig.(4). From the measured values, they concluded (ignoring diffusion and shear modulus change with temperature) that at lower temperature regime over-coming of Peierls stress is   rate controlling. Nevertheless at high temperature they did not rule out the possibility of dislocation climb as   rate controlling.

Then Schmidt and Whitley (42) during their study on lamellar Al-CuAl$_2$ composite, they measured the stress expo-nent value separately on CuAl$_2$. The n value is 4.5. The creep rate of CuAl$_2$ falls in a steep manner from 10^{-4}/sec. at 400°C to 10^{-8}/sec at 325°C.
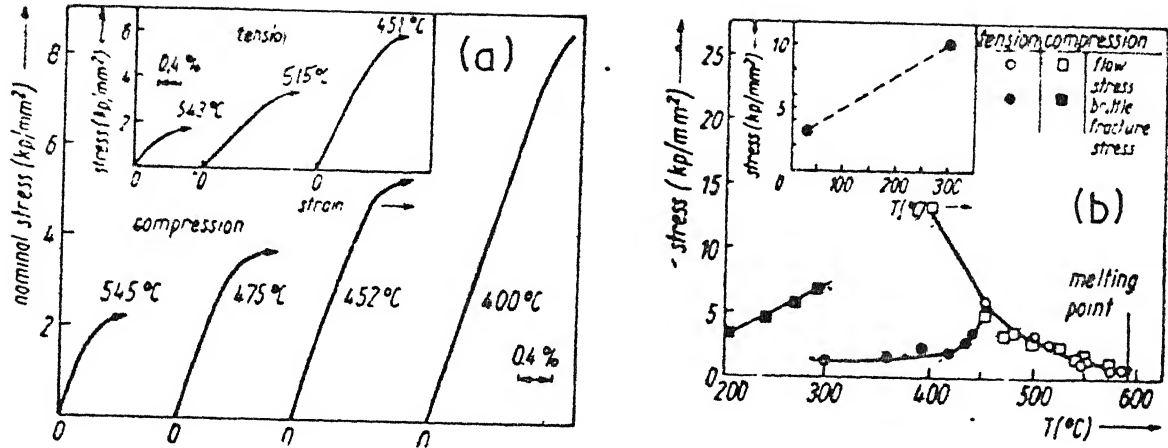
Fig. 4. (a) Stress-strain curves under compression ($\dot{\varepsilon} = 10^{-3}\text{s}^{-1}$).
Inset shows results for a tension specimen .
(b) Variation of flow stress with temperature ($\dot{\varepsilon} = 10^{-3}\text{s}^{-1}$).
Inset shows the ultimate compression strength
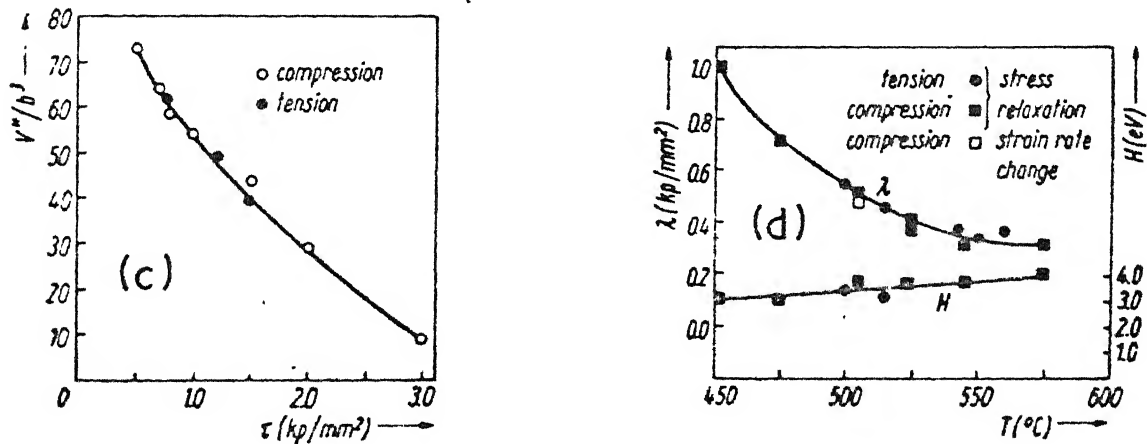
Fig. 4 (c) Activation volume as a function of applied stress for $CuAl_2$.
(d) Strain rate sensitivity and activation enthalpy as a function
of temperature for $CuAl_2$.

1.3 SCOPE OF THE PRESENT WORK

In recent years the emerging technology has seen a rapid development of new high strength materials. In the process of exploring high strength materials, it has been observed that intermetallic compounds have many outstanding properties compared to metals and alloys. However, their brittleness has caused a big barrier in using them as structural materials. Nevertheless this problem has been overcome in some intermetallics. The polycrystalline brittleness has been ascribed to high Peierl stress, restricted cross slip, a large slip vector, limited number of slip systems and difficulty of transmittal of slip across grain boundaries. However, before polycrystalline ductility can be improved, it is necessary to note whether single crystals of the same are ductile or not.

Firstly, the single crystal ductility and the effect of temperature on it have been investigated in this study. Secondly, the effect of grain size on the ductile - brittle transition temperature has been studied. Further, the effect of introducing mobile dislocations through a small amount of pre-strain at an appropriate temperature has been explored. Finally an attempt has been made to identify the flow mechanism by assessing the thermally activated flow behaviour. It is of interest to understand the factors affecting the ductile-brittle transition in order to overcome their brittleness and thereby utilize them as structural materials.

CHAPTER - II

EXPERIMENTAL PROCEDURE

2.1 PROCESSING DETAILS AND METALLOGRAPHY

(a) Alloy Preparation :

In the present investigation the Cu-Al alloy of nominal composition 53.5 wt % Cu and 46.5 wt % Al was prepared by making use of Cu and Al both of 99.9% purity. These metals were melted in a vacuum induction furnace in a high purity graphite split mould (fig. 5a) under a vacuum better than 2×10^{-2} Torr. The alloy so obtained was crushed into small chunks and remelted making use of the mould b (fig. 5b). In this manner six rods of 7 mm dia and 8 cm length were obtained. Two batches of alloys and rods were prepared and their chemical analysis indicated the compositions as 53.8 wt % Cu (batch 1) and 53.2 wt % Cu (batch 2).

The powder from each batch was also analysed by X-Ray powder diffraction method. The intensity versus angle data are presented in Fig.(6) and the peaks were indexed making use of ASTM data file for $CuAl_2$.

In addition to the as cast condition, single crystal and P/m (powder metallurgy) specimens were also prepared for subsequent mechanical testing.
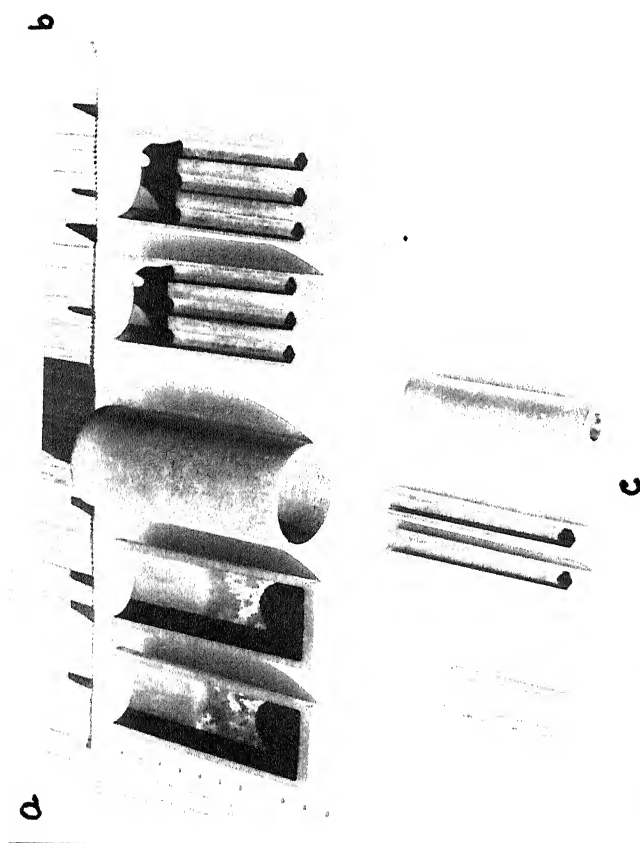
Fig. 5. Photograph of :

(a) graphite split mould used for melting
(b) graphite split mould used for preparing rods
(c) graphite split mould used for preparing single
    crystals
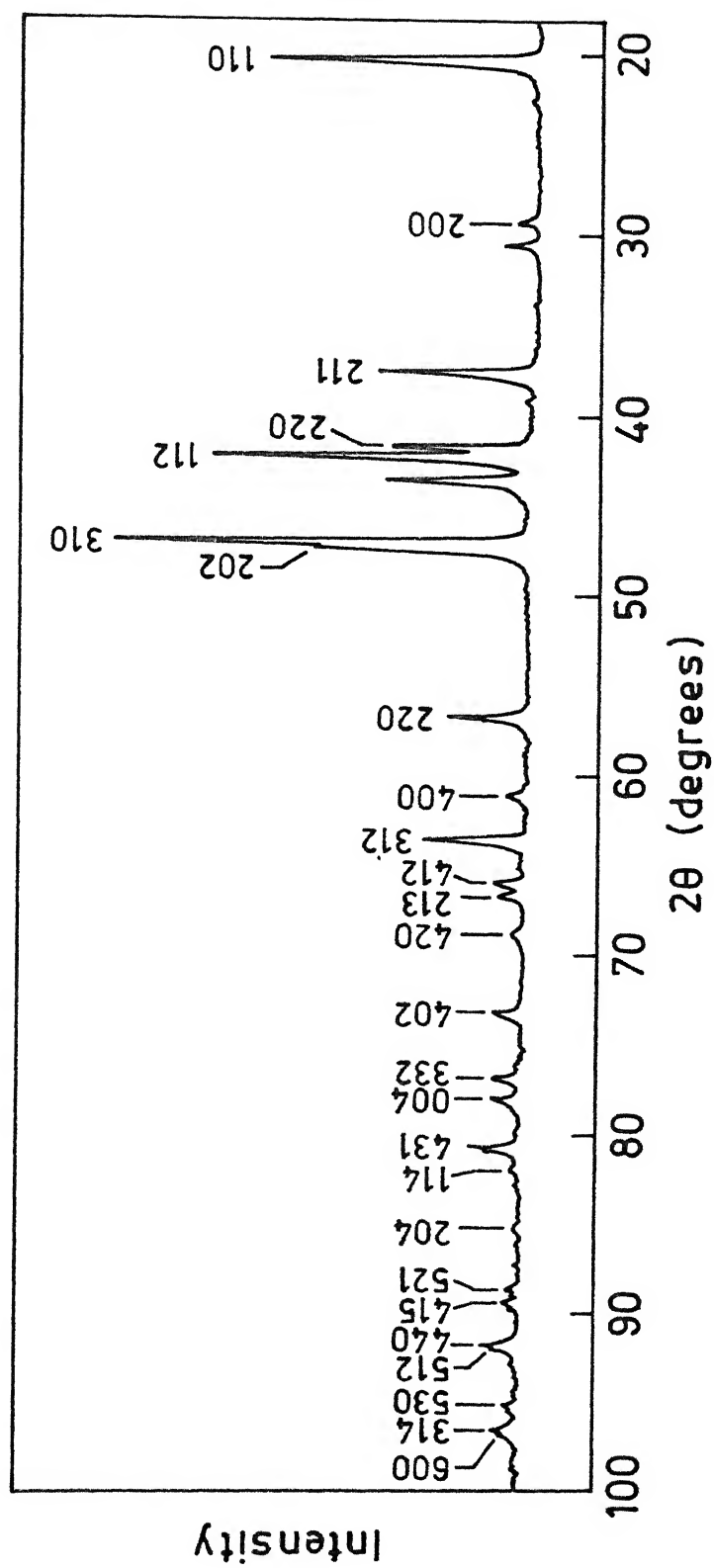
Fig. 6. X-ray diffraction pattern of CuAl$_2$ sample (radiation CuK$_\alpha$ with Ni filter).

(b) <u>Preparation of single crystals</u>

Some of the cast rods were fitted in another graphite split mould (fig.5c) and single crystals were grown by Bridgeman technique under a vacuum of 10^{-1} Torr. In this set-up, the furnace was stationary while the crucible was lowered into the furnace at a rate ranging from 0.75 cm/hr. to 1.75 cm/hr. The photograph of the apparatus is given in fig.(7).

The rods so obtained were examined for grain boundaries, if any by macro-etching with $FeCl_3$ etchant. Laue back reflection technique was employed to confirm the absence of grain boundaries. However, the Laue photographs were not indexed for orientation determination. A Laue photograph is shown in Fig.(8).

(c) <u>Processing details of powder metallurgy (P/m)</u>

In order to obtain a very fine grain size, the P/m technique was adopted. First the cast ingot was broken into small pieces (below 3 mm size) in an agate crucible. Then these chunks were transferred to the Ball mill. The balls (10 mm dia) were made off tungsten carbide. The ball weight to feed weight was chosen as 4. After 24 hours of grinding in acetone medium, the powder was taken out by decanting the vessel in a beaker and then heated at 100°C for 2 hours in an oven. The particle size analysis was carried out on a sample of powder and the size analysis is shown in the form of a bar chart Fig.(9). The powder
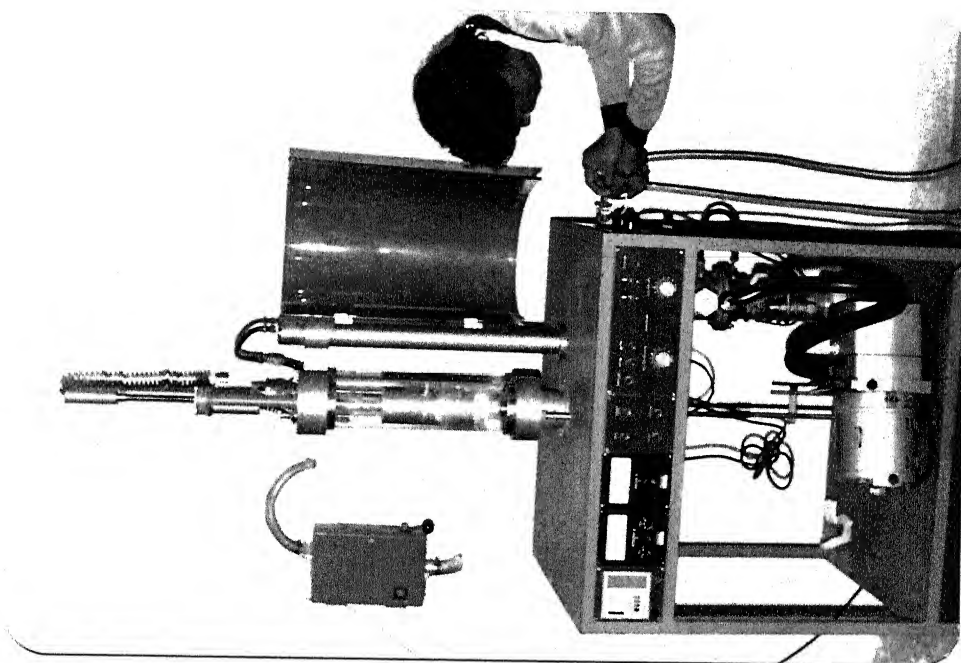
Fig.7. Photograph of the apparatus for crystal growth (Bridgman – Czockralski methods).
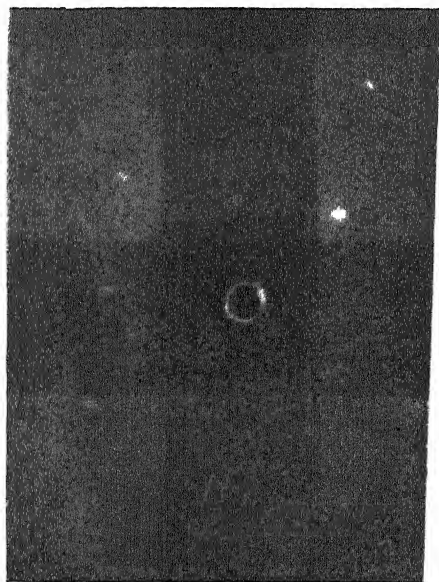
Fig. 8. A typical Laue-back-reflection
pattern of a single crystal rod.
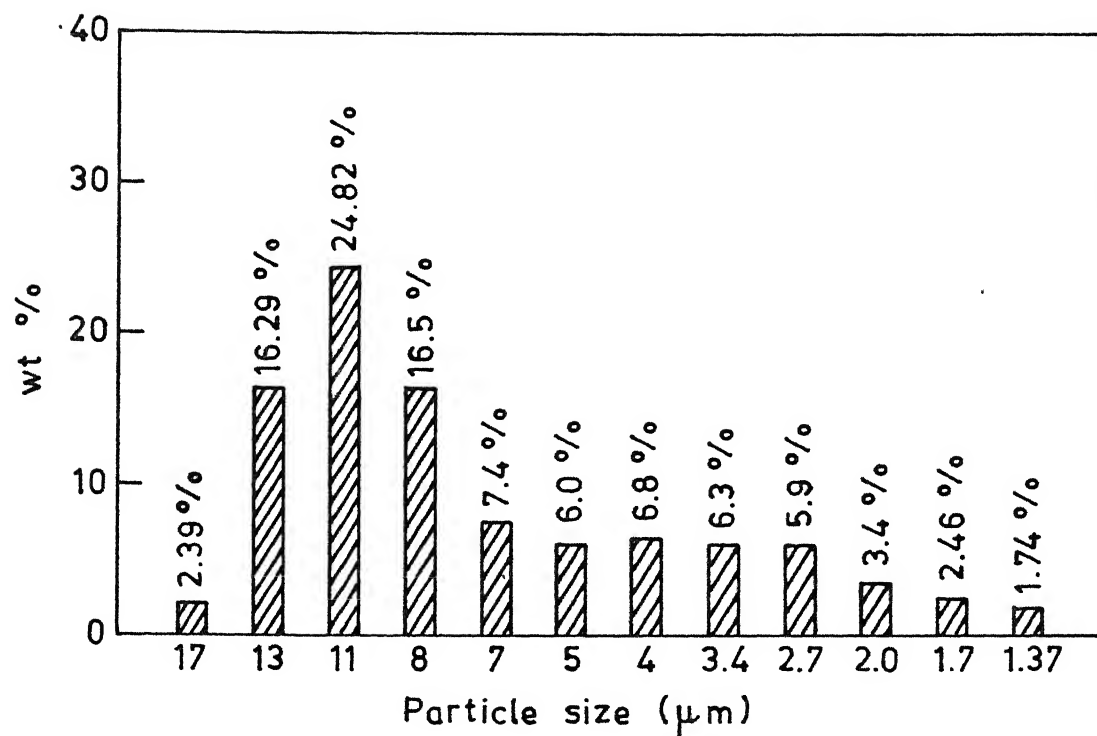
Fig. 9. Bar chart of wt % vs particle size of the CuAl$_2$ powder prepared by ball milling.

was hot compacted making use of a graphite die. The photograph of the whole hot compaction set-up is given in Fig.(10).

In order to assess the porosity, the density was measured by Xyline impregnation method. The density of various specimens was in the range of 95% to 99% of the theoretical density (4.34 gm/cc).

(d)   Compression specimen preparation

Cast and single crystal cylindrical specimens (dia 7 mm, ht. 7.7 to 8.0 mm) were prepared for compression testing using a diamond (automated Bueheler CO) saw. The cut surfaces of the specimens were lightly ground and polished to obtain smooth and parallel surfaces. Since the P/m specimens were already in the required size for compression testing their top and bottom surfaces were ground and polished.

(e)   Metallography

The metallographic specimen preparation involved standard procedures of grinding and polishing followed by electrolytic polishing and electrolytic etching. The following conditions were employed :

(1) electrolyte : solution of HNO_3 and CH_3OH in 1:2 proportion

(2) Cathode   : stainless steel

(3) Voltage   : 1-2 volts

(4) temperature : 0°C
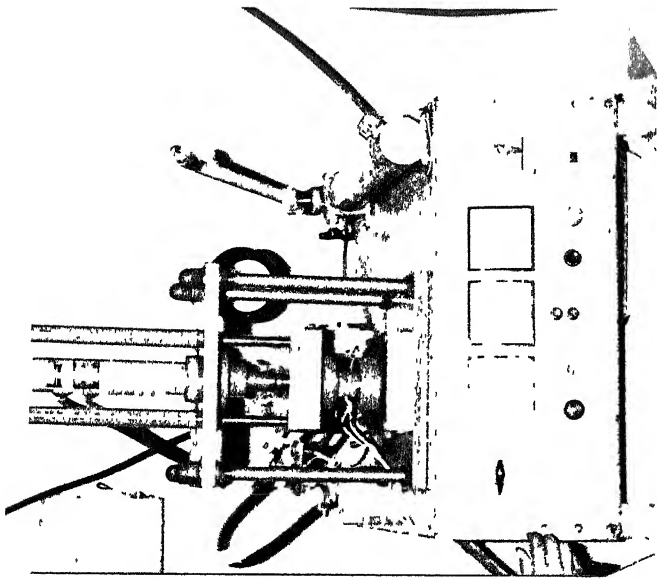
Fig. 10. Photograph of the hot compaction set—up for P/m specimen preparation.

The grain size measurement was done by linear intercept technique. These values have been reported with the micrograph.

2.2 TESTING DETAILS

All the tests were performed on an M.T.S. m/c with specially prepared compression Jig (Fig.(11)). The compression test was carried out in the temperature range of 275°C to 575°C with the help of a resistance furnace. The temperature was controlled with three thermocouples kept very close to the sample. The temperature was controlled within $\pm$ 2°C from the required test temperature. The tests were carried out in stroke control mode. The end friction between the specimen and platen was minimised by making use of Al_2O_3 (1 μm) powder as lubricant. In the course of our investigations, mainly three types of tests were performed, namely constant cross head speed, change of temperature at constant cross head speed and change of cross head speed at a given temperature.

(a) Constant cross head speed test

This type of test was done on a sample upto fracture in order to assess the ductility and flow curve at each temperature. The strain rate is given by the following expression :

$$= \frac{d\varepsilon}{dt} = \frac{1}{L_o} \times \frac{\Delta L}{\Delta t}$$ where L_o is the gauge length

of the test specimen.
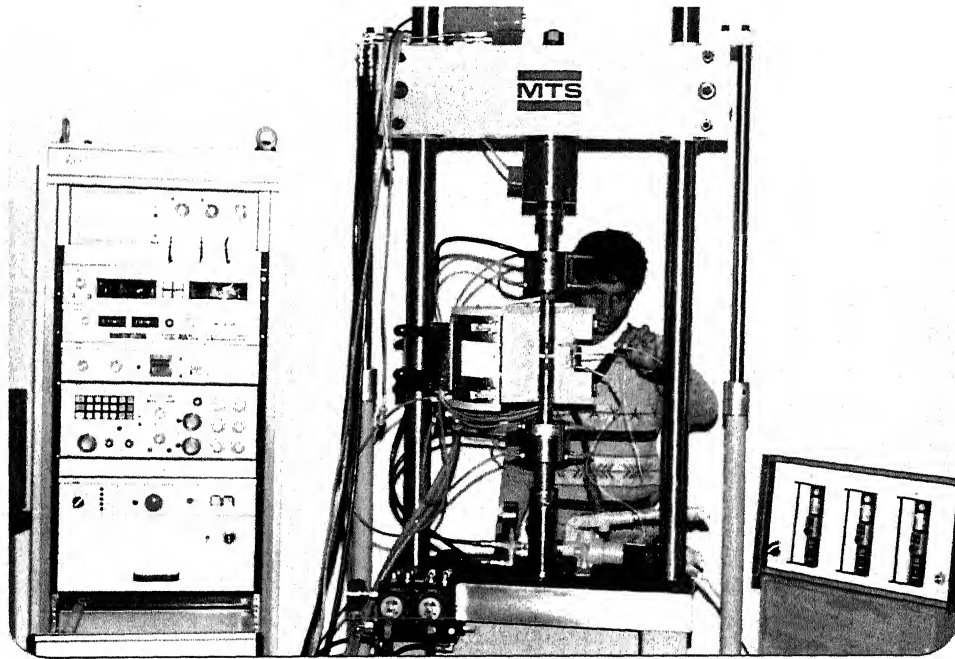
Fig. 11. Photograph of the whole M.T.S. machine
with specially prepared compression Jigs.

Noting that $L_o = 8$ mm and $\dot{\varepsilon} = 5 \times 10^{-5}$ sec^{-1}, the time needed for 10 mm displacement is 2.5×10^4 sec. This time is set in rate meter I of the MTS machine by manual operation in order to obtain a strain rate of 5×10^{-5} sec^{-1}. The range of temperature in which this type of test was done is 325°C to 575°C.

(b)   Change of temperature test at constant cross head speed

The flow stress variation with temperature was assessed by this type of test. In this test, a specimen is deformed first at 575°C upto a small plastic strain ($<1\%$) and then the temperature is successively lowered and the same kind of test is repeated on the same sample upto a lower temperature of 325°C. A temperature interval of 25°C is chosen for this purpose. Each time the test is started after a period of 10 minutes following the temperature stabilization.

(c)   Change of cross head speed test

Under this category two different types of test were done,   namely single cross head speed change and multiple cross head speed change.

(i) Single cross head speed change :- This type of test was done for obtaining data of activation volume, deformation activation energy and strain rate sensitivity. The starting temperature was

575°C for each type of specimen. The specimen is deformed to a small plastic strain (1%), then the cross head speed is changed by a factor of 10 i.e. from $= 5 \times 10^{-5}$ sec^{-1} to 5×10^{-4} sec^{-1}. After a small amount of plastic strain ($<1\%$) at the second strain rate the specimen was unloaded and the temperature was set for next lower temperature. This type of test was repeated upto 325°C. The strain rate change test was also performed at various strain levels on single crystal and P/m specimens at different temperatures.

(ii) <u>Multiple across head speed change</u> : In order to determine the stress exponent (n), this type of test was performed. The cross head speed was changed in steps of a factor of 10 on a single specimen after about 0.5% plastic strain. This test was performed in the increasing order of cross head speed, covering a strain rate range of 5×10^{-5} sec^{-1} to 5×10^{-2} sec^{-1}. This type of test was carried out at 475°C and 575°C on single crystal and P/m specimens.

CHAPTER III

RESULTS

Experimental results are divided into two broad sections, dealing with ductility and flow curve on the one hand and identification of flow mechanism through the calculation of activation parameters on the other. The factors considered for this purpose are (i) the effect of grain size variation, (ii) the nature of the boundaries and (iii) mobile dislocations.

3.1   Part I

3.1.1   EFFECT OF GRAIN SIZE

Widely different grain sizes were obtained through processing. These include single crystals, specimens in the as cast condition and specimens processed by P/m route. In addition to these categories, other grain sizes were obtained through recrystallization of initially single crystals and also the cast specimens. In order to recrystallize the specimens, they were subjected to a prestrain of about 10% at 575°C. Thus the specimens with various grain sizes were tested at a constant cross head speed at various temperatures in order to assess the flow curves and ductility.

The microstructures of the specimens were also examined by the optical microscopy before and after the testing to see the effect of testing conditions on microstructural stability. A minor grain growth was noticed in P/m samples (Fig.(17)), whereas

both cast and single crystal specimens have undergone a considerable change through recrystallization. Although no systematic study was done in this regard Fig. (12) to fig. (16) indicate that after deformation the grain size had changed. Also single crystals did not remain as single crystals Fig.(15) especially when deformed at 575°C. This fact was utilised to study the effect of fresh boundaries arising from recrystallization on strength and ductility. Actually both cast and single crystal specimens were deformed at 575°C to 10% strain - Fig.(12), (14) & (15) show that new grains (78 um,109um,80 um) were formed after this treatment on cast and single crystal specimens respectively after 10% strain. Fig.(19) shows the effect of grain size variation on stress-strain curves at different temperatures. Initially there is some strain hardening followed by strain softening. The cast and single crystal specimens have extensive strain softening region, whereas in P/m very minor amount of strain softening is observed. But the degree of work hardening in P/m specimen is more compared to other two types. At all temperatures, the strength of P/m specimens is the highest among all.

The onset of ductility can be assessed from the plot of fracture strain versus temperature. (Fig.20) Both single and P/m specimens are brittle upto 375°C after which the fracture strain increases rapidly. In the cast specimen the brittle-ductile transition takes place at 400°C. However, the ductility of P/m specimens at 575°C and 525°C is lower than that of as cast and single crystal specimens. The P/m specimens fractured in shear mode all three temperatures after extensive deformation - Fig. (18).

Fig. 12. Microstructure following deformation of cast sample at 575°C.X160(d=78 μm).

Fig.13. Microstructure following deformation of cast sample at 525°C X500 (d=25 μm).

Fig.14. Microstructure following prestraining (10%) at 575°C and subsequent deformation at 525°C of a single crystal. X125 (d= 109 μm).

Fig.15. Microstructure following deformation of single crystal at 575°C X200 (d=80 μm).
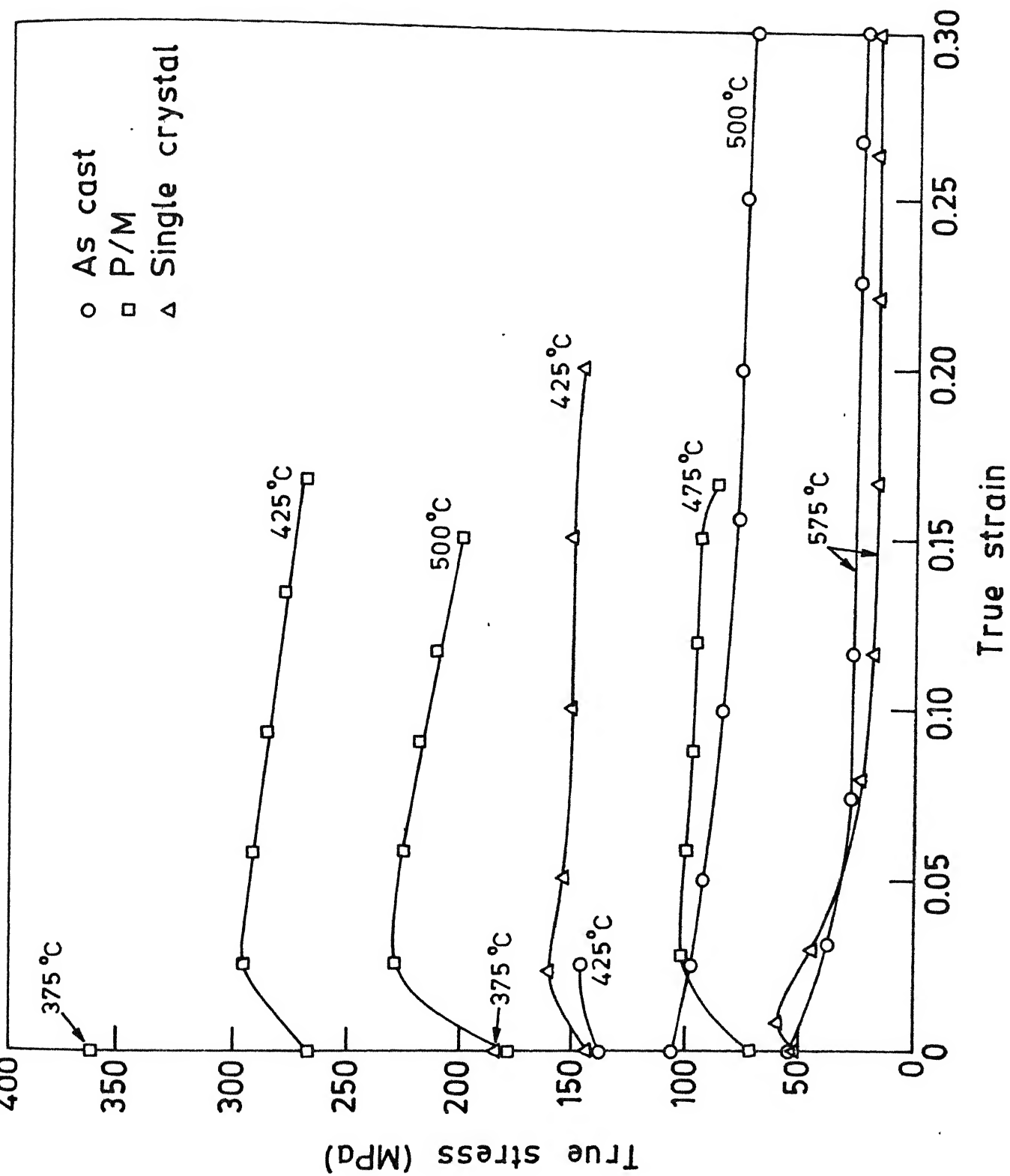
Fig. 19. Plot of true stress vs true plastic strain for various samples ($\dot{\varepsilon} = 5 \times 10^{-5}\,s^{-1}$) at different temperatures.
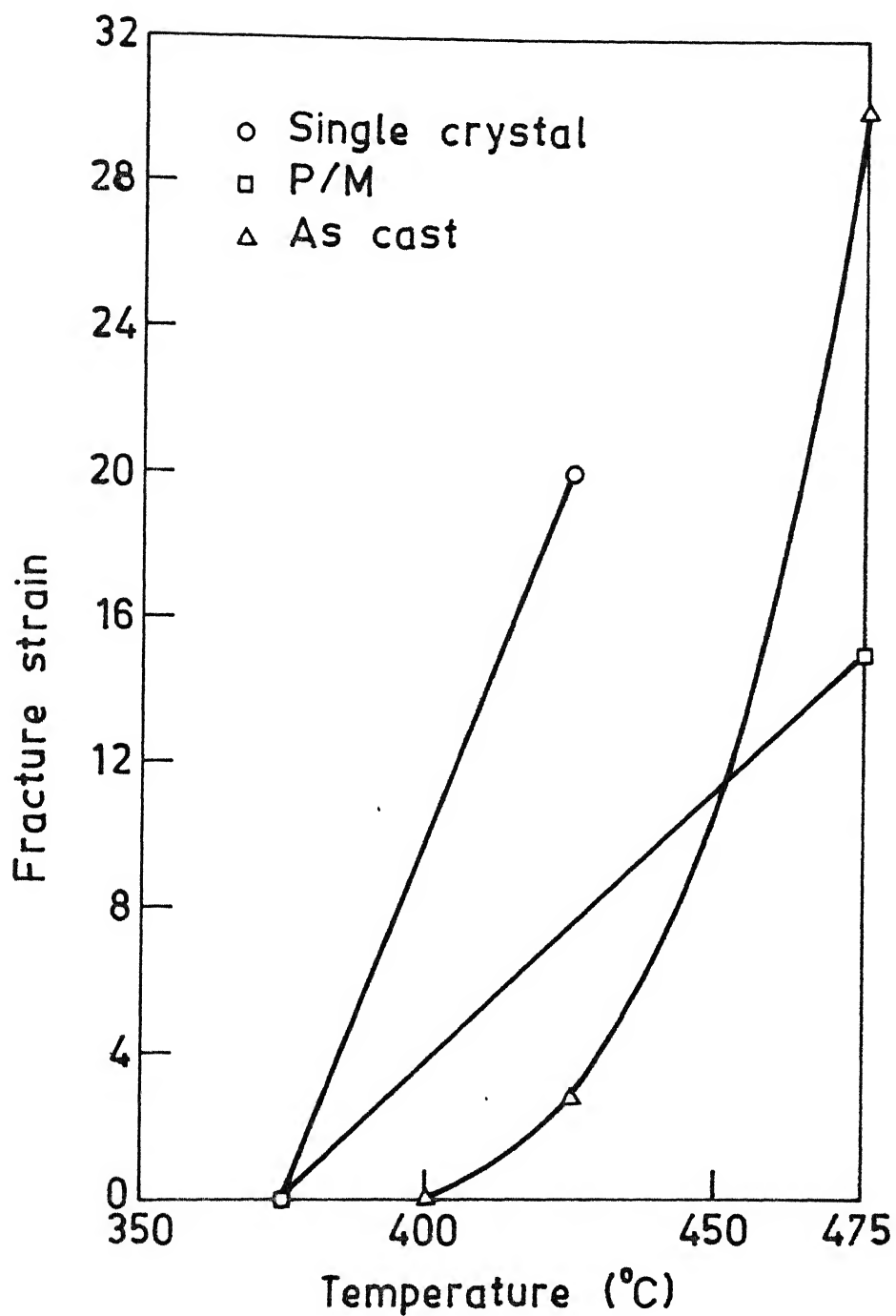
Fig. 20. Fracture strain vs temperature diagram of various samples ($\dot{\epsilon} = 5 \times 10^{-5} s^{-1}$).

3.1.2 THE EFFECT OF NATURE OF BOUNDARIES

To study the effect of change in boundary structure both single crystal and as cast specimens were deformed at 575°C to a 10% plastic strain level and the structure was examined. The fig.(12) to Fig. (16) suggest that extensive recrystallization has taken place. Then these recrystallized specimens were tested at other temperatures and their flow behaviour is compared with others.

(a) Comparison of recrystallized versus as-cast

The recrystallized specimens failed in a brittle manner at 375°C whereas at 420°C, the specimens of the same kind undergo extensive deformation. At 450°C and at 525°C, the as cast specimen has higher yield stress although at 525°C they are pretty close to each other.In terms of ductility the as cast specimen has higher amount both at 450°C and 525°C. It is seen that strain softening occurs in all cases(Fig.21).

(b) Comparison of single crystal versus recrystallized

The single crystal fails in a brittle manner upto 375°C. Nevertheless at 425°C a lot of ductility is apparent in the fig.(22). The single crystal at all temperatures shows a small work hardening portion, whereas it is absent in the recrystallized specimen.
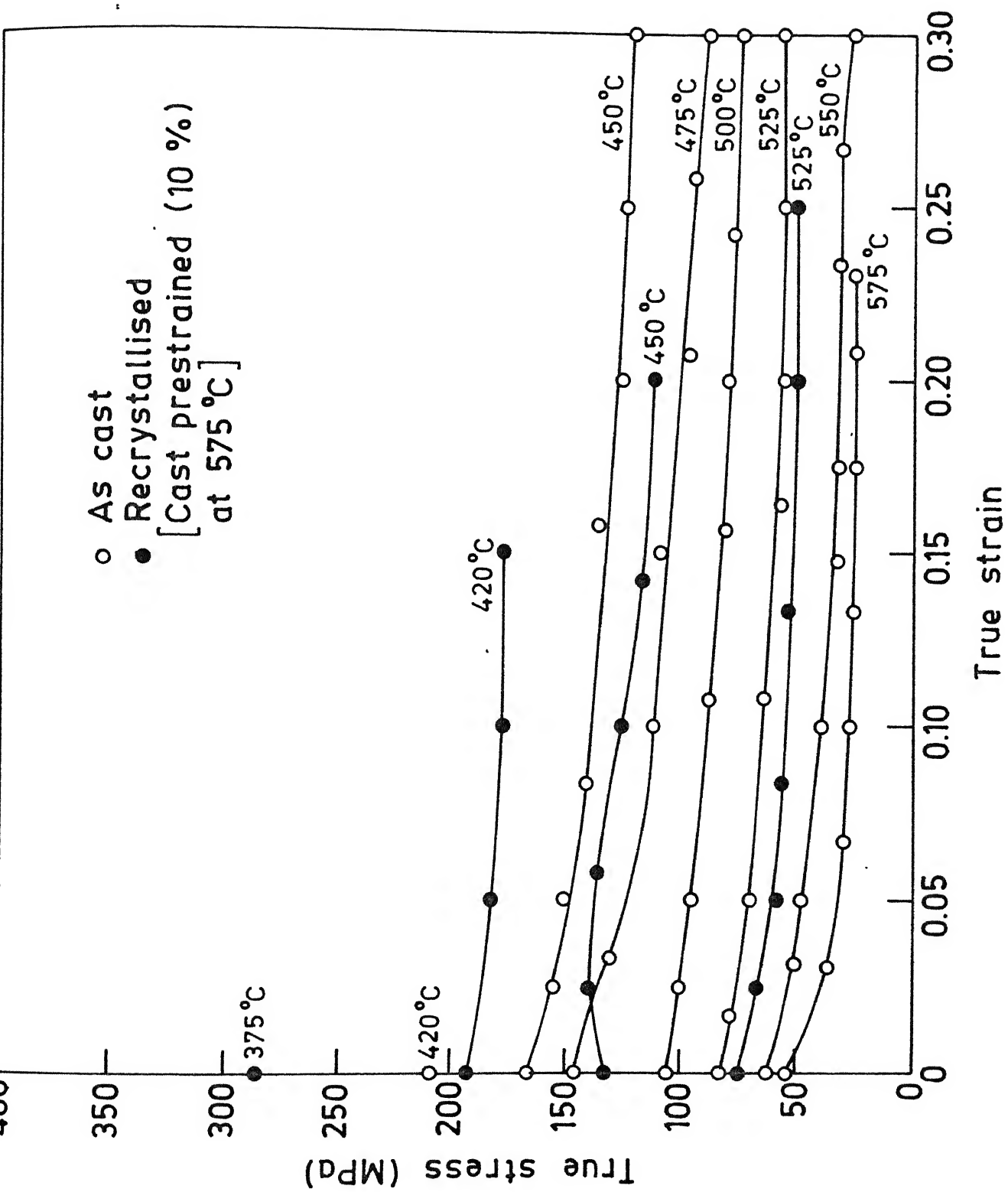
Fig. 21. True stress vs true plastic strain diagram of as cast and recrystallised specimens at different temperatures ($\dot{\epsilon} = 5\times10^{-5} \, s^{-1}$).
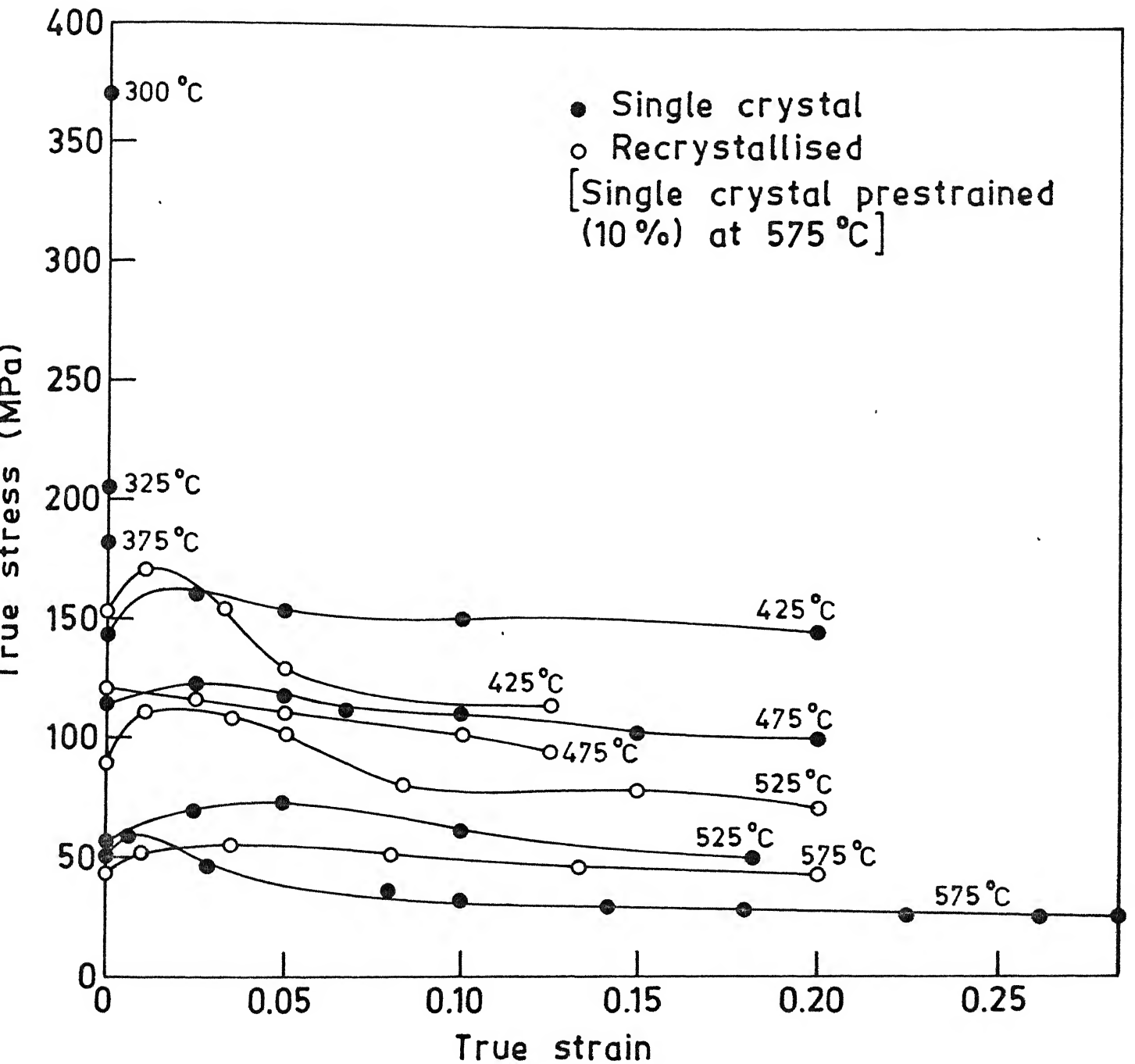
Fig. 22. True stress vs true plastic strain diagram of the single crystal and recrystallised specimens tested at different temperatures ($\dot{\varepsilon} = 5 \times 10^{-5} s^{-1}$).

Both types of sample show considerable amount
of strain softening. The yield strength of recrys-
tallized specimen is higher at all temperatures
(425°C, 475°C, 525°C) other than 575°C. Based on
the observation of edge cracking tendency of both
types of samples, it is worth mentioning that at
575°C the single crystal has a higher ductility.
Nevertheless at test temperatures of 425 and 475°C
the single crystal has higher ductility. At 575°C
the recrystallized specimen fractured in shear mode
as shown in Fig. (18).

3.1.3 Effect of introduction of mobile dislocations

To study this effect the following method was
adopted. Both single as well as cast specimens were deformed
to a 3% strain at 475°C. Then microstructure of both type of
samples were examined by optical microscopy. There was no
evidence of recrystallization as a consequence of the above
treatment. Then both the types of specimens were tested at
lower temperatures. The data on as cast specimens are compared
with the same, following the prestrain and single crystals are
compared with single crystals after prestrain.

3.1.3(a) Comparison of single crystal with and without prestrain

Fig. (23) shows typical σ - ε curves illustrating the
effect of pre-strain. The single crystals are found to be brittle

Fig. 23. True stress vs true plastic strain diagram of single crystal specimens ($\dot{\epsilon} = 5 \times 10^{-5} s^{-1}$) at different temperatures.

upto 375°C whereas 4% ductility has been achieved in the pre-strained specimen at the same temperature. Also the brittle fracture stress of the prestrained specimen is higher at test temperatures of 325°C and 375°C. However, at 425°C, the yield stress is same in both types of specimens.

3.1.3(b) Comparison of Cast Specimen with and without Prestrain

Fig.(24) shows typical curves illustrating the effect of prestrain. Because of the limited data, the comparison can be made only at 425°C. At 425°C ductility of the order of 2.5% is apparent from the figure whereas 19% ductility is achieved through prestraining. Moreover at 325°C, 1% ductility has been achieved in the prestrained specimen. The cast specimen fails in a brittle manner at 400°C. At 375°C, the prestrained specimen shows extensive ductility of the order of 17.5%. The yield strength can be compared only at one temperature i.e. 425°C. The prestrained specimen has much higher yield strength compared to its counterpart at the same temperature.

3.1.4 The Effect of Temperature on flow stress of various specimens

Fig.(25) shows a typical flow stress versus temperature plot of various samples. It is seen that at a particular temperature, the P/m specimen has the highest and single crystal has the lowest flow stress. Flow stress changes almost linearly in all four kinds of samples with temperature.
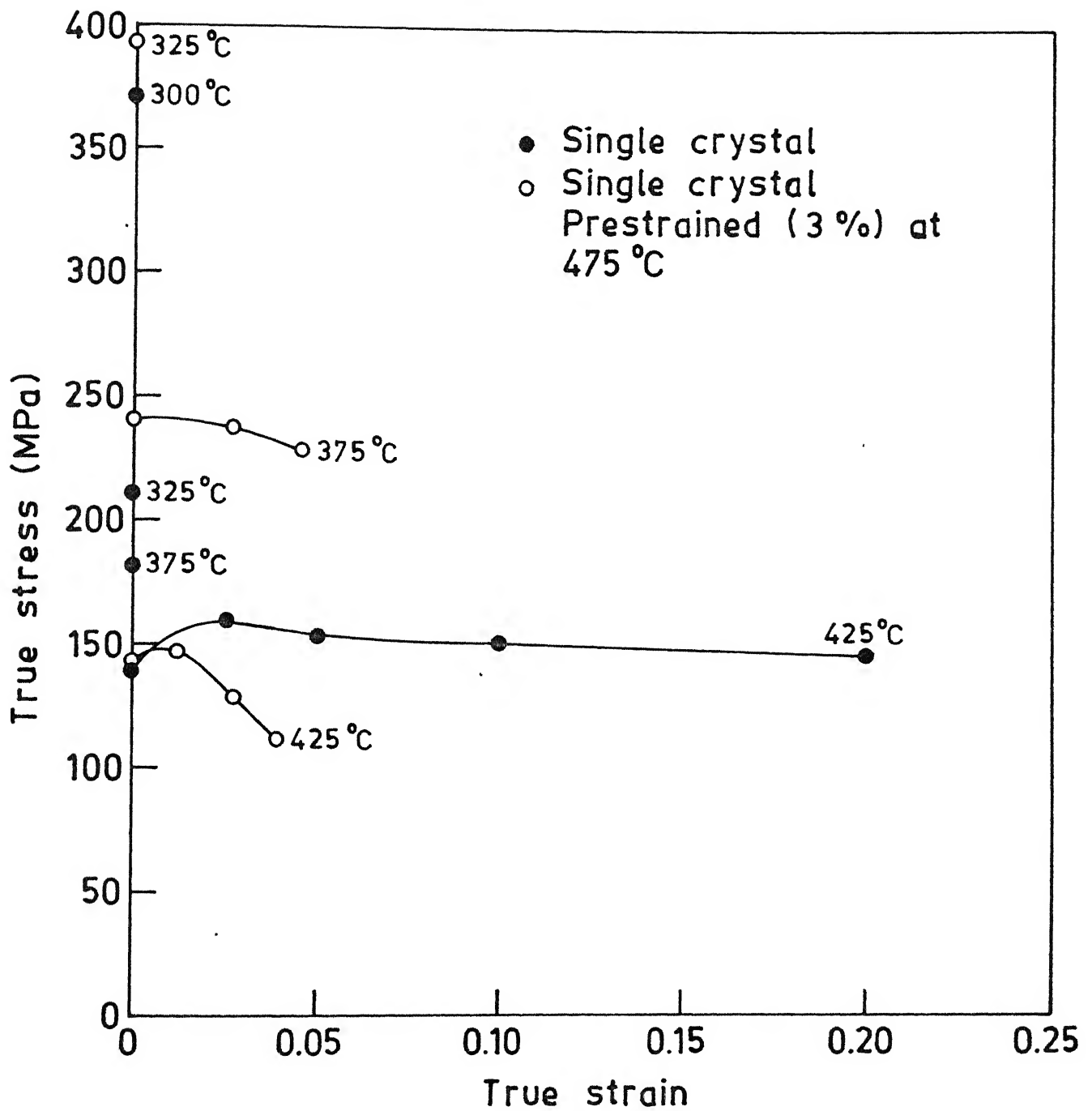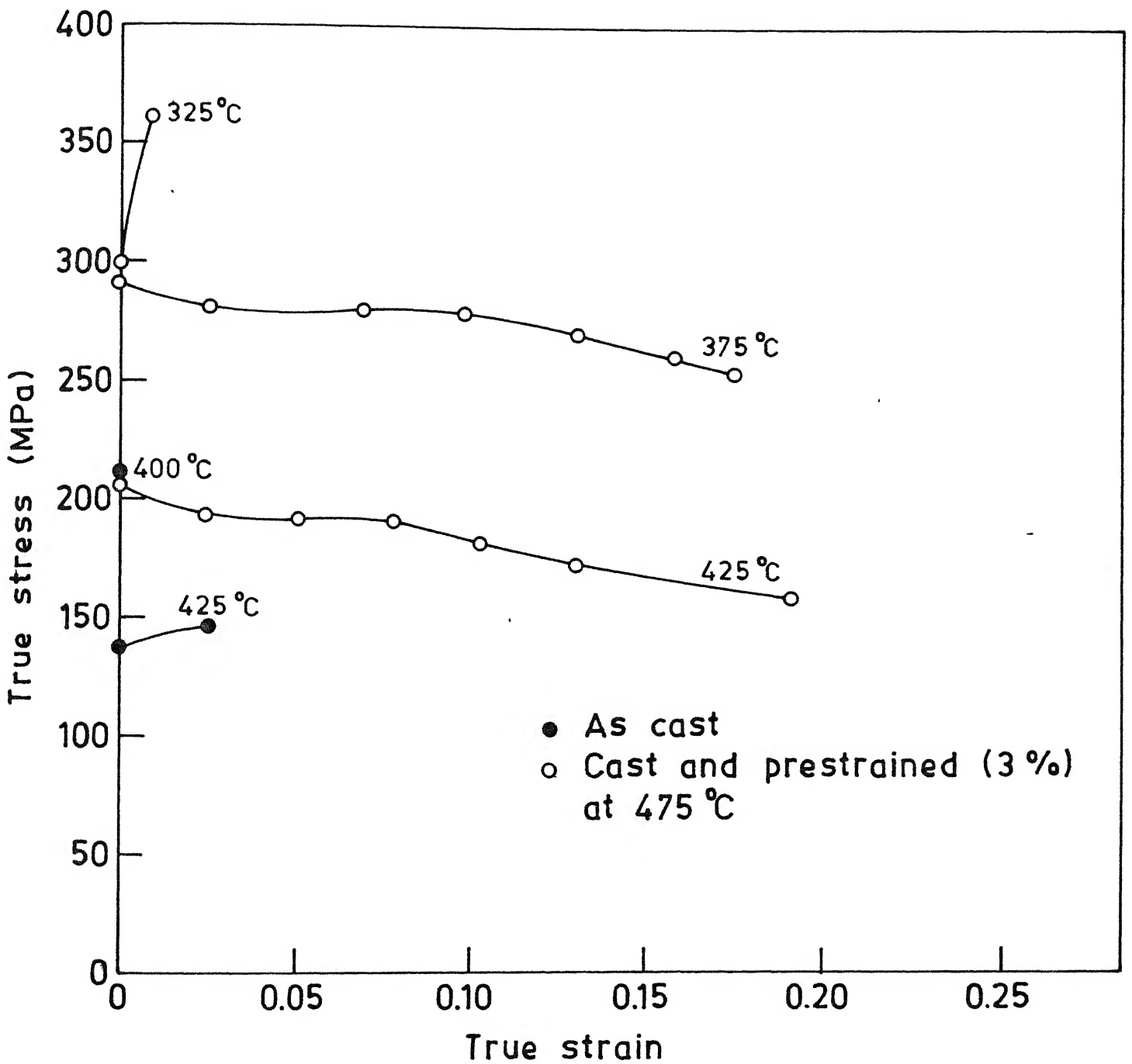
Fig. 24. True stress vs true plastic strain diagram of as cast specimens ($\dot{\epsilon} = 5 \times 10^{-5} s^{-1}$) at different temperatures.
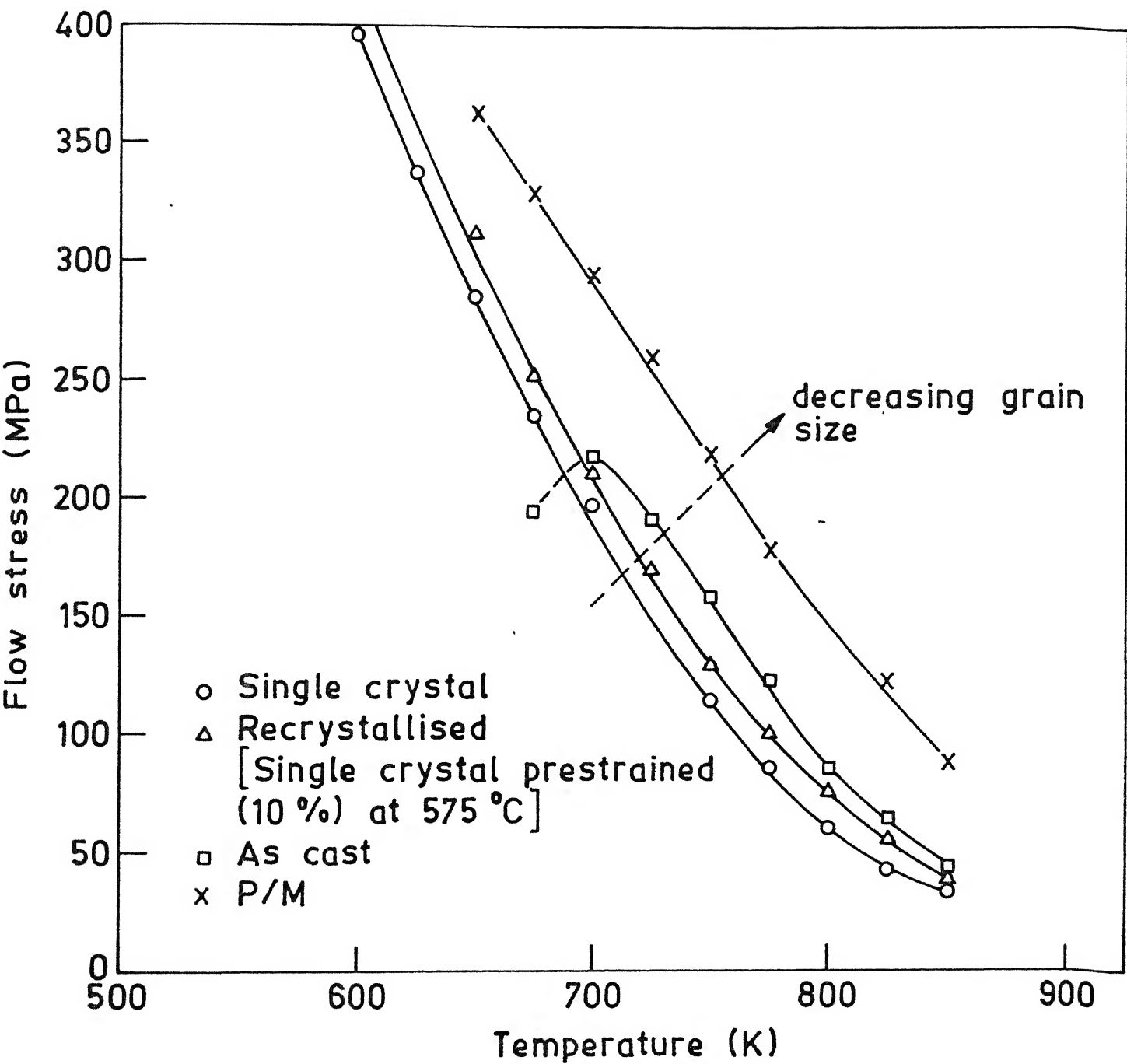
g. 25. Plot of flow stress vs temperature for various samples ($\dot{\epsilon} = 5 \times 10^{-5} s^{-1}$)

3.1.5 The Effect of Temperature as well as Grain size variation

It is well known that above .5 Tm (Tm = melting points) the diffusion plays a prominent role in metals and alloys. Further, finer grain size leads to a lower strength compared to coarser grain size at elevated temperatures. On the other hand, flow stress increases with decreasing grain size at lower temperatures.

Fig.(26) shows that as the grain size decreases the flow stress increases and the trend continues from 400°C to 575°C which is close to the melting point (M/p.591°C).Moreover, the slope is almost constant over the whole temperature range.

3.1.6 S U M M A R Y

(1) The ductile-brittle transition temperature of as cast $CuAl_2$ is 400°C,whereas it is 375°C for P/m and single crystal specimens. No systematic grain size effect can be inferred from these observations. Also ductile brittle transition temperature of as cast material is 400°C, whereas recrystallized specimens exhibited transition temperature of 375°C.

(2) Work hardening tendency and yield stress are highest in P/m specimens over the whole temperature range.
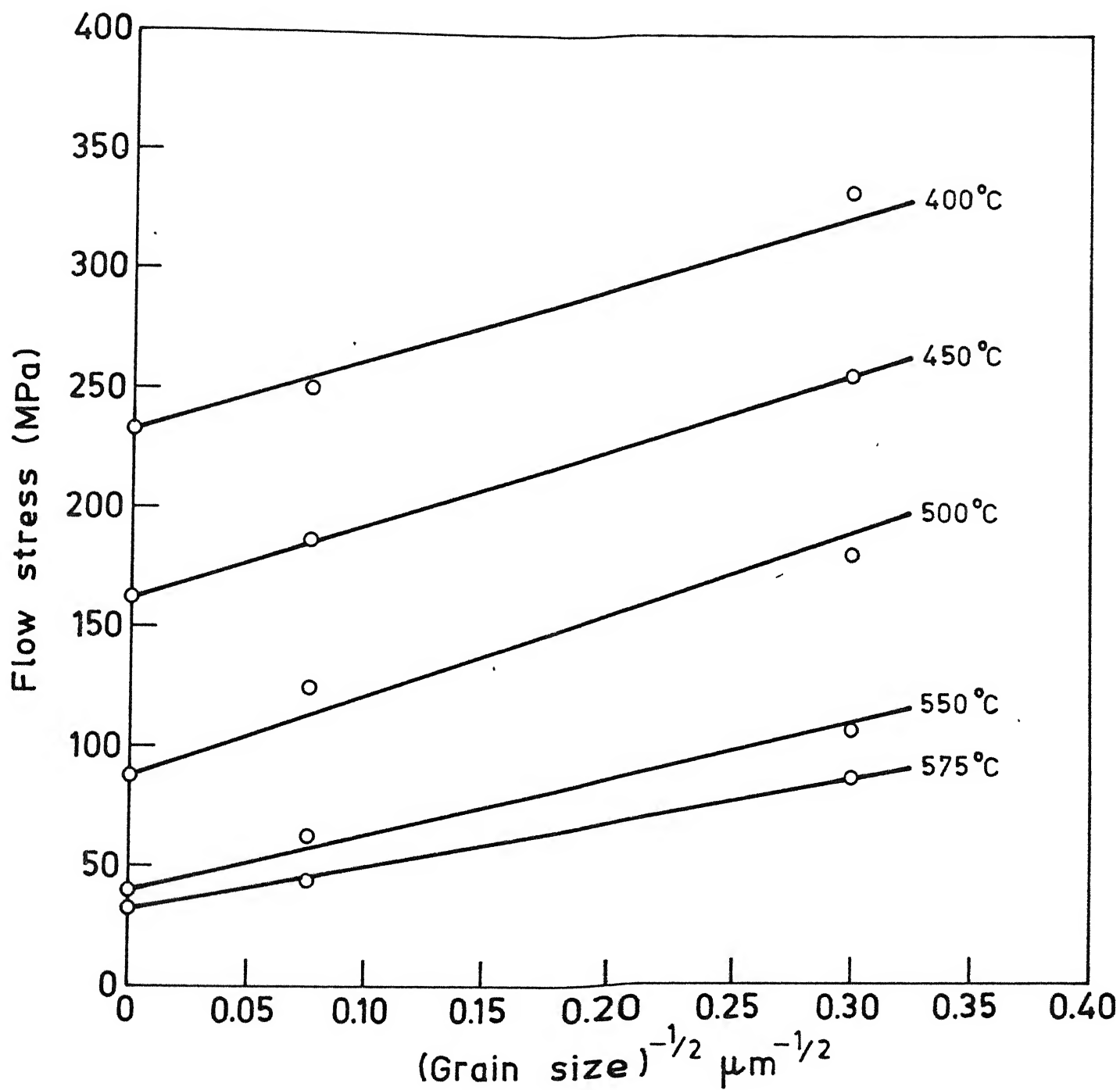
Fig. 26. Flow stress vs (grain size)$^{-1/2}$ diagram at various temperatures ($\dot{\epsilon} = 5 \times 10^{-5} s^{-1}$).

(3) The ductility of P/m specimens is the lowest at 500°C and 575°C.

(4) At temperatures 425°C, 500°C and 575°C, the P/m specimens fractured in shear mode after extensive deformation whereas both the single crystal and as cast specimens failed by edge cracking.

(5) The specimens recrystallized starting from single crystals fractured in shear mode at 575°C and 525°C.

(6) The as-cast specimen has higher ductility and yield strength both at 450°C and 525°C, compared to its counters part.

(7) The yield strength of recrystallized specimen (single crystal prestrained (10%) at 575°C) is higher at all temperatures compared to its counterpart.

(8) The ductile-brittle transition temperature is lowered as a result of introducing mobile dislocation in single crystals.

(9) The ductile-brittle transition temperature is lowered to 325°C as a result of introducing mobile dislocations into the cast specimens whereas it is 400°C for the as cast condition.

(10) Flow stress changes almost linearly with temperature in all types of samples. At a particular temperature, the P/m specimens have the highest flow stress while single crystal has the lowest. This trend is observed over the whole temperature range.

(11) Hall-Petch relation is found to be valid over the whole temperature range upto 575°C.

3.2   PART -II

Plastic deformation is the consequence of the movement of dislocations through the crystal lattice. The fact that significant stress is needed to induce plasticity implies that the dislocations encounter obstacles. The temperature dependence of the yield stress in metals suggests that thermal fluctuations can supply energy to assist the motion of the dislocations past the obstacles. Plastic deformation of crystalline solids is considered to be thermally activated. The obstacles are of two types (a) short range ex-forces due to forest dislocations, assymetric point defects, Peierls-Nabarro barrier i.e. alternate low and high energy configuration of dislocation core, (b) long-range forces due to dislocations on parallel slip planes, grain boundaries, large second phase particles etc.

The interaction force increases rapidly in case of short range obstacles and effective over a small area of slip plane whereas the interaction force changes slowly with the position of the dislocation and it is not very sensitive to temperature.

In general both types of obstacles are present in the lattice and the applied stress (σ) is given by $\sigma = \sigma_{\mu} + \sigma^*$ where σ_{μ} = Athermal component of flow stress and σ^* = thermal component of flow stress. The plastic strain rate is given by $\dot{\varepsilon} = Pb\bar{v}$ .... (1), where $\dot{\varepsilon}$ = true plastic strain rate.

$\qquad$ P = density of mobile dislocations

$\qquad$ b = Burger's vector

$\qquad$ $\bar{v}$ = the average velocity of dislocations.

Since the motion of dislocations past obstacles is thermally activated,

$$\dot{\varepsilon} = \dot{\varepsilon}_0 \exp - \left(\frac{G'}{KT} \right) \ \text{....... (2)}$$

where $\dot{\varepsilon}_0 = NAb\nu$, G' = Gibb's free energy of activation,

$\qquad$ K = Boltzmann constant,

$\qquad$ T = temperature in absolute scale,

$\qquad$ N = number of activation sites per unit volume,

$\qquad$ A = area swept out per successful fluctuations

$\qquad$ P = mobile dislocation density,

$\qquad$ ν = frequency factor $= \dfrac{\nu_D \cdot b}{L}$

and $\quad$ b = Burger's vector.

The exponential term arises from the fact that the velocity of a dislocation will be limited by the probability that a dislocation will successfully overcome an obstacle under the externally applied stress when thermally activated. Equation (2) is the general expression for the low temperature thermally activated plastic flow of crystalline solids and its applicability is independent of any specific deformation mechanism.

where,

∂D = Debye frequency

L = length of dislocation involved in activation.

The equation (2) can be written as -

$$\dot{\varepsilon} = \dot{\varepsilon}_0 \; exp.- \; (\frac{H - TS}{K \; T})$$

where H is enthalpy and S is entropy of activation :

or,

$$\dot{\varepsilon} = \dot{\varepsilon}_0 \; exp \; (\frac{S}{K}). \; exp-(\frac{H}{KT})$$

or $\dot{\varepsilon} = \dot{\varepsilon}_0^{o'} \; exp \; - \; (\frac{H}{KT})$

where $\dot{\xi}_0^{'} = \dot{\varepsilon}_0 \; exp(\frac{S}{K})$

So,

$$H = KT \; ln(\frac{\dot{\varepsilon}_0^{'}}{\dot{\varepsilon}_0}) \; \dots\dots \; (3)$$

hence apparent activation energy varies linearly with temperature. Application of an effective stress σ^* moves the dislocation up the barrier to a position x_1, under a force $F^* = \sigma^*.b.L$

To move to a position X_2, the dislocation
has to traverse a distance d^*. So the energy
needed for that purpose is the H.

So $H = H_0$ - work done by applied stress = $H_0 - \sigma^* \, b \, d^* . L^*$

$$= H_0 - V^* . \sigma^*$$

where, $V^* = bd^* . L^*$ = activation volume. ....(4)

d^* = barrier width, L^* = length of the dislocation
involved in the activation.

So $V^* = \dfrac{\partial H}{\partial \sigma^*}$ ....(5)

3.2.1. Evaluation of the Activation volume (V^*)

From eq.(3). $\ln \dot{\varepsilon} = \ln \dot{\varepsilon}_0 - \dfrac{H}{KT}$

Combining (3) and (5)

$$V^* = KT \left[\ln \left(-\dfrac{\dot{\varepsilon}}{\dot{\varepsilon}_0}\right) \Big/ \partial \sigma^* \right] \, T.$$

If $\dot{\varepsilon}_0'$ is constant.

then V^* $KT\left(\dfrac{\Delta \ln \dot{\varepsilon}}{\Delta \sigma^*}\right)_T \simeq KT \left[\dfrac{\ln \left(\dfrac{\dot{\varepsilon}_2}{\dot{\varepsilon}_1}\right)}{\Delta \sigma^*} \right]_T$ .....(5a)

or, $V^* \simeq KT \left[\dfrac{\partial \ln \dot{\varepsilon}}{\Delta \sigma^*} \right]_T$

Thus the effect of sudden change in $\dot{\varepsilon}$ on flow stress
at a given test temperature would yield activation volume (V^*).
The activation volume data thus calculated are presented in
Fig.(27). It is seen from Fig.(27) that V^* is sensitive neither
to temperature nor to the grain size. Fig.(28) also suggests
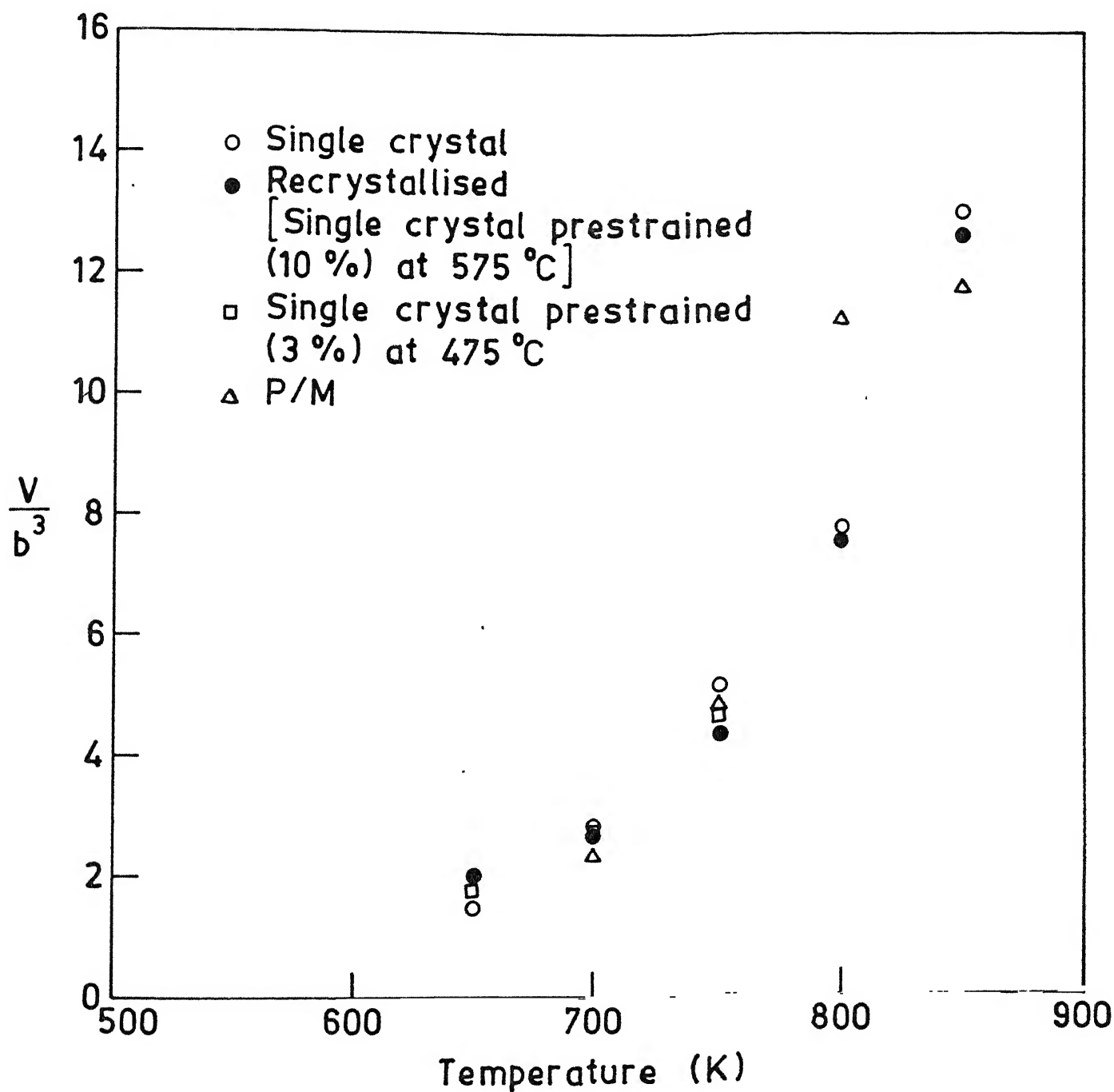that V^* does not vary with plastic strain.

Fig. 27. Activation volume vs temperature diagram for various samples (b = atom size).
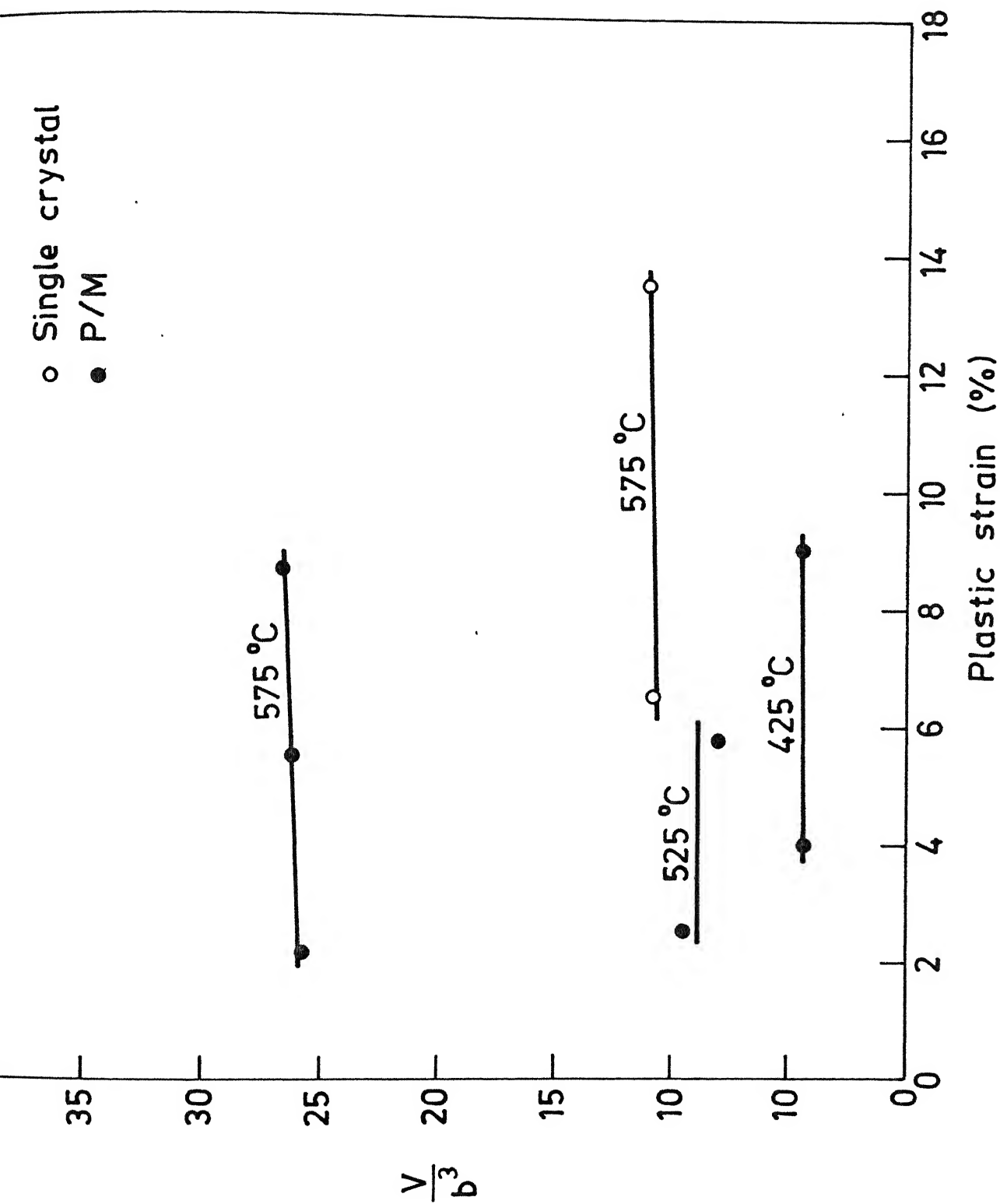
Fig. 28. Activation volume vs plastic strain diagram at various temperatures (b = atom size)

3.2.2 Evaluation of Apparent activation energy (H)

Combining eqn.(3) and (4), we have

$$H_0 - V^* \sigma^* = KT \ln \frac{\dot{\varepsilon}_0{}'}{\dot{\varepsilon}} \quad \ldots\ldots\ldots (6)$$

differentiating equation (6) with respect to T for constant $\dot{\varepsilon}$

$$-V^* \cdot \frac{\partial \sigma^*}{\partial T}\bigg|_{\dot{\varepsilon}} = K \ln \frac{\dot{\varepsilon}_0{}'}{\dot{\varepsilon}}$$

$$V^* = - \frac{K \ln \left(\frac{\dot{\varepsilon}_0{}'}{\dot{\varepsilon}}\right)}{\frac{\partial \sigma^*}{\partial T}}\bigg|_{\dot{\varepsilon}} \quad \ldots\ldots\ldots (7)$$

From equation 5(a) and (7)

$$V^* = KT \left(\frac{\partial \ln \dot{\varepsilon}}{\partial \sigma^*}\right)_T = -K \frac{\ln\left(\frac{\dot{\varepsilon}_0{}'}{\dot{\varepsilon}}\right)}{\frac{\partial \sigma^*}{\partial T}}\bigg|_{\dot{\varepsilon}}$$

$$\therefore \frac{\ln \dot{\varepsilon}}{\partial \sigma^*}\bigg|_T = -\frac{1}{T} \frac{\ln\left(\frac{\dot{\varepsilon}_0{}'}{\dot{\varepsilon}}\right)}{\frac{\partial \sigma^*}{\partial T}}\bigg|_{\dot{\varepsilon}}$$

$$\text{or} \quad \ln\left(\frac{\dot{\varepsilon}_0{}'}{\dot{\varepsilon}}\right) = -T\left(\frac{\partial \sigma^*}{\partial T}\right)_{\dot{\varepsilon}} \left(\frac{\partial \ln \dot{\varepsilon}}{\partial \sigma^*}\right)_T \quad \ldots\ldots\ldots (8)$$

Substituting equation (8) in equation (3)

$$H = -KT^2 \cdot \left(\frac{\partial \sigma^*}{\partial T}\right)_{\dot{\varepsilon}} \left(\frac{\partial \ln \dot{\varepsilon}}{\partial \sigma^*}\right)_T$$

$$\text{or,} \quad H = -T \cdot \left(KT \cdot \frac{\partial \ln \dot{\varepsilon}}{\partial \sigma^*}\right)_T \left(\frac{\partial \sigma^*}{\partial T}\right).$$

$$\text{or,} \quad H = -T \cdot V^* \left(\frac{\partial \sigma^*}{\partial T}\right)_{\dot{\varepsilon}} \quad \ldots\ldots\ldots (9)$$

Thus the apparent activation energy H can be calculated from V^* and the slope of σ^* vs T curve at a given temperature.

The activation energy thus calculated is plotted as a function of temperature for various specimens (Fig.29). It is seen that H varies linearly with temperature and at any particular temperature the P/m specimen has the highest activation energy.

3.23. Evaluation of Strain rate Sensitivity (m)

In the high temperature deformation the flow stress (σ) - strain rate ($\dot{\varepsilon}$) relation can usually be expressed as

$$\sigma = K \dot{\varepsilon}^{m} \quad \ldots\ldots\ldots (10)$$

where K and m are constants 'm' is known as strain rate senstivity index. We have that

$$m = \frac{\ln \dfrac{\sigma_2}{\sigma_1}}{\ln \dfrac{\dot{\varepsilon}_2}{\dot{\varepsilon}_1}} = \frac{\ln (P_2/P_1)}{\ln (v_2/v_1)} \quad \ldots\ldots\ldots (11)$$

where P is load and v is cross head speed. Making use of equation (11), the strain rate senstivity index can be determined. Such data as a function of temperature are shown in Fig.(30). Among all the specimens, the P/m specimens can be seen to be exhibiting lower m values.

Plots of flow stress versus strain rate obtained by the strain rate change test are shown in Fig.(31). Only two temperatures (475°C and 575°C) were chosen for this purpose. Moreover, these tests were performed on single crystal and P/m specimens. The stress exponent (n) value is calculated from
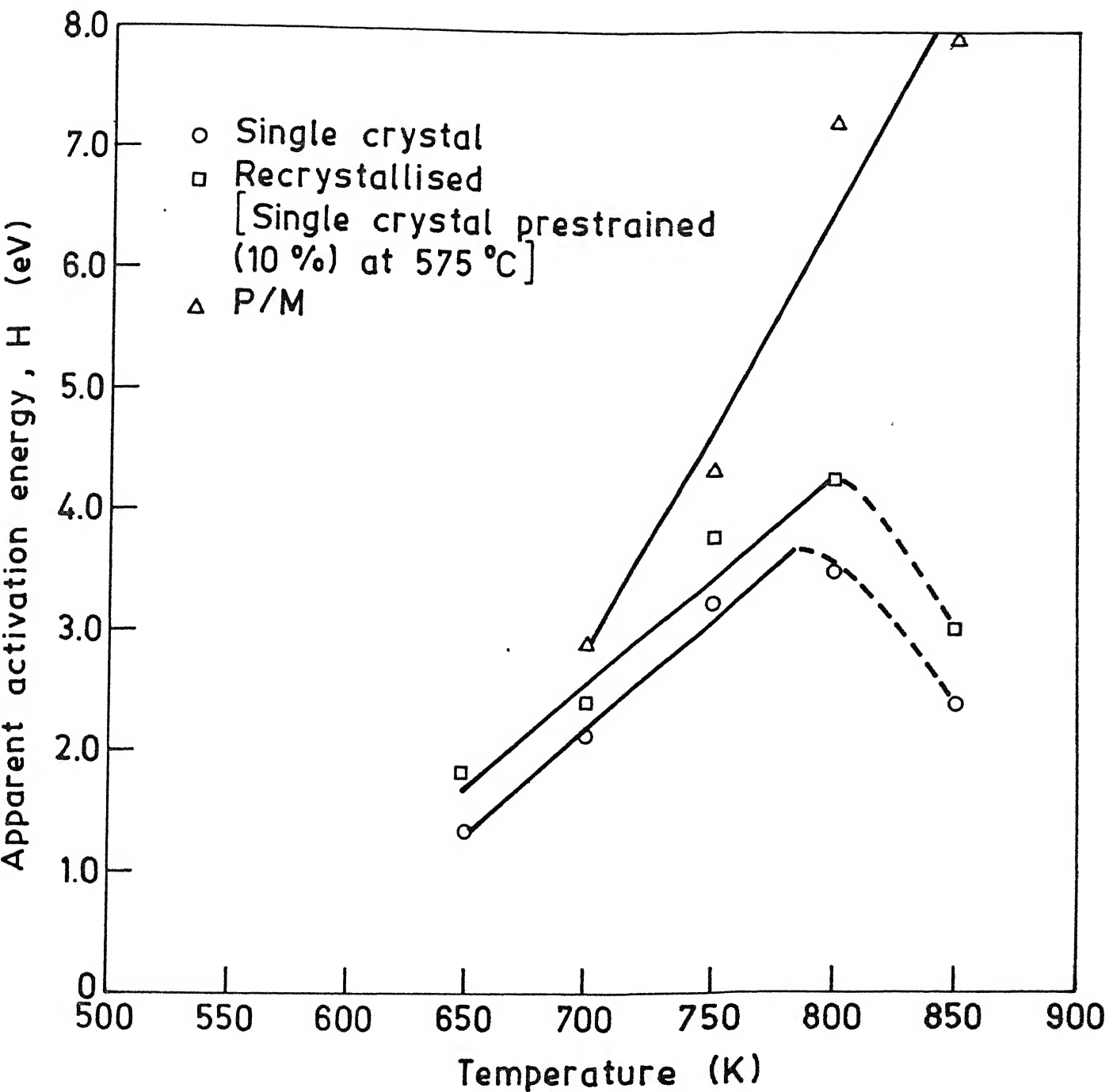
Fig. 29. Apparent activation energy vs temperature diagram of various specimens.
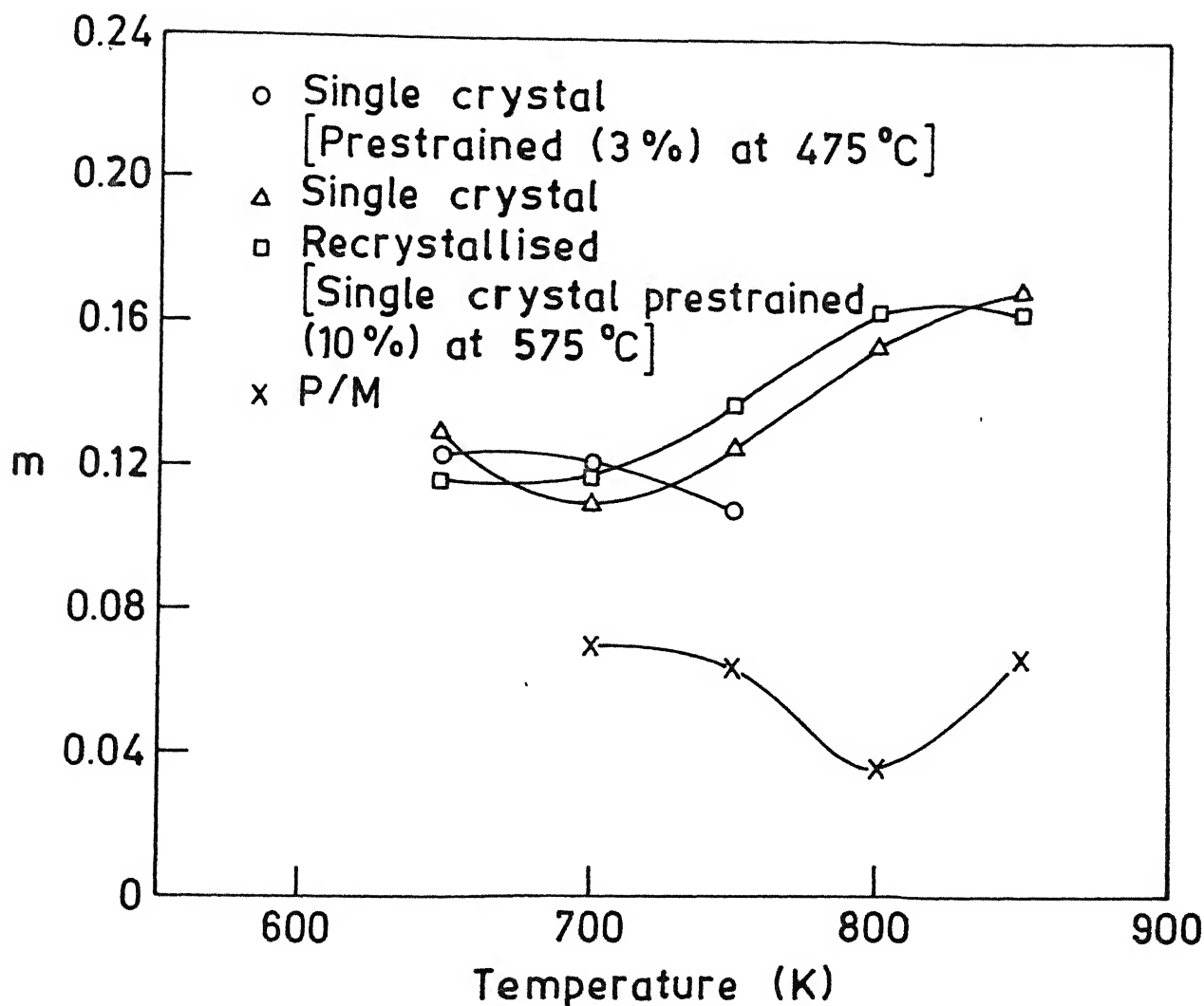
Fig. 30. Strain rate sensitivity vs temperature diagram for various samples.
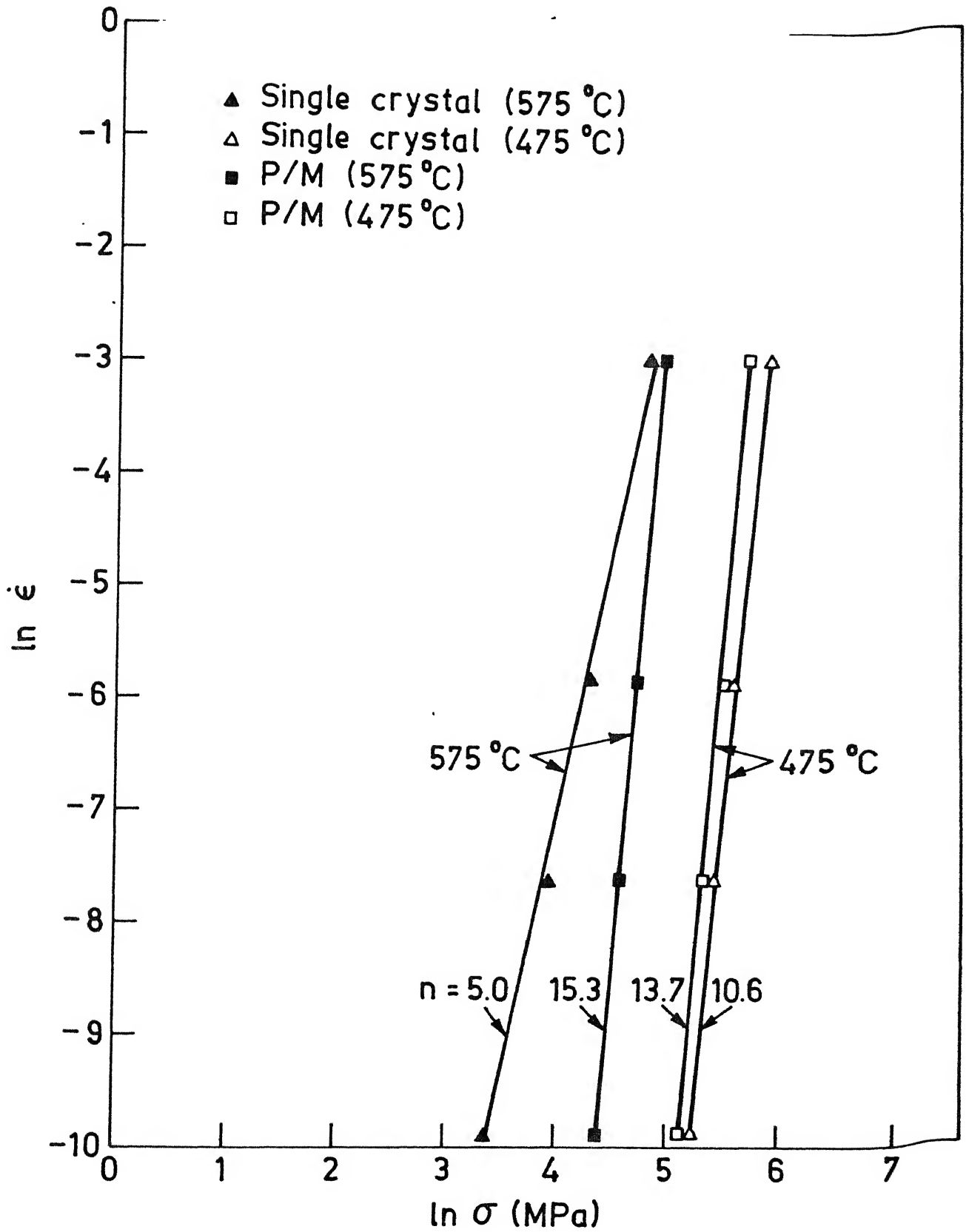
Fig. 31. Plot of strain rate vs stress at elevated temperatures.

the slope of double logarithmic plots. The deformation acti-vation energy (Q) was also calculated using the Dorn equation for high temperature creep considering the data at constant strain rate.

$$\dot{\varepsilon} = K \, \sigma^n \, \exp - (\frac{Q}{RT}) \, \ldots\ldots\ldots \, (12)$$

The value for P/m sample is estimated as 5.38 eV.

CHAPTER IV

D I S C U S S I O N

The discussion concerning the ductility and strength
of single crystals versus polycrystals and identification of
flow mechanism will be considered.

4.1 DUCTILITY AND STRENGTH

4.1.1 SINGLE CRYSTALS

From the figure (20), it is apparent that the brittle-
ductile transition temperature is 375°C. In this connection
the work of Kirsten (39) on single crystal ductility of $CuAl_2$
might be mentioned for comparison. Kirsten found that cleavage
faces of $CuAl_2$ deformed at 400°C showed asterism in the Laue
pattern which signified some deformation at 400°C. He observed
that above 500°C $CuAl_2$ deformed plastically.

In agreement with our results, Ignat and Durand (40)
studied the slip system of single crystals under compression
creep behaviour in the temperature range of 400°C to 450°C and
at stresses from 10 to 40 MN/m^2 through slip trace technique.
It can thus be inferred that at 400°C the single crystals are
ductile.

The transition from brittle to ductile behaviour as
the temperature is increased can be expected when the yield
stress is lower than the fracture stress. This can arise due
to strong temperature sensitivity of the yield stress.

The stress strain curves (Fig.19) show initial rise in flow stress followed by a drop with increasing strain. The initial increase in flow stress (strain hardening) is attributable to rise in dislocation density on loading. This strain hardening effect continues for a short strain interval and recovery processes set in quickly due to high temperature of testing. The subsequent drop in stress is attributable to the continuing recovery of the initial high density dislocation structure till the material attains a stable structure through polygonization or recrystallization. Once the structure is stabilized the flow continues at a constant stress level provided fracture does not set in and interfere with steady state flow.

4.1.2 POLYCRYSTALS

The B.D.T. temperature of P/m specimens is 375°C, whereas for cast specimens, it is 400°C. We may mention here some previous observations on $CuAl_2$ for comparison. Dey & Tyson[15] found that polycrystalline $CuAl_2$ deformed above 400°C under compressive load and above 450°C under dynamic tensile load.

The P/m specimens have the highest strength and work hardening capacity over the whole temperature range. These can be ascribed to its smallest grain size and high capacity of dislocation accumulation.

4.1.3. COMPARISON OF SINGLE CRYSTAL AND POLYCRYSTALLINE BEHAVIOUR

Both single crystal and P/m specimens have the same B.D.T. temperature despite the extreme variation in their grain size. From this observation, it can be inferred that above 375°C the desired five independent slip systems are there for polycrystalline ductility. Also the grain size variation does not seem to play any role in shifting the transition temperature.

However, the B.D.T. temperatures for as cast (400°C) and single crystal specimens (375°C) are different. The plausible reason could be due to the grain boundary segregation which may lead to embrittlement.

But considering all the three together one can say that there is no systematic change in B.D.T. temperature with grain size variation. But it can also be inferred that the extent of sensitivity of B.D.T. temperature with grain size variation is very low.

In general, it is found that single crystals have lower strength when compared to polycrystals over the whole temperature range. This is normal due to the grain boundary strengthening effect over the whole temperature range. However, a few exceptions in this regard could be due to orientation differences, as no attempt has been made to fix the orientation of all single crystal specimens.in this study.

4.1.4 SMALL PRESTRAINING(3%) EFFECT

The B.D.T. temperature is lowered significantly on pre-straining the single crystal and as-cast specimens. The increase in mobile dislocation density seems to be responsible for this effect.It is interesting to note that both the strength and ductility are simultaneously increased by increasing the mobile dislocation density.

4.2 IDENTIFICATION OF MECHANISM

The low temperature deformation behaviour of metals and alloys is generally interpreted as a consequence of either interaction of dislocations with defects or lattice frictional stress. The common thermally activated mechanism and their characteristics are shown in Table (a)(43).

Table (a)

Mechanism	Magnified of V^*	Characteristics
Peierls-Nabarro	$1-10^2 b^3$	V^* independent of strain, H_o is related to the energy required to nucleate a double kink
Forest – dislocations	$10^2-10^4 b^3$	V^* decreases, and τ^* increases with strain as forest dislocation density increases
The motion of jogs in screw dislocation	$10-10^3 b^3$	H_o equals self diffusion energy, V^* depends on strain as thermal jog spacing increases, or intersection jog spacing increases.
Point defect drag	$1-10^3 b^3$	H_o given by migration energy of point defect.
Point defect interaction	$1-10^2 b^3$	V^* is related to concentration of point defect controlling deformation. V^* may depend on strain.
Cross slip of screw dislocation	$10-10^2 b^3$	Often rate controlling for extended dislocation, H includes a construction term.
Climb of edge dislocation	$1 b^3$	H_o equals self diffusion energy. $\dot{\gamma} \propto \tau^n$ where n = 4.5.

Table (a) Contd...

Mechanism	Magnified of V^*	Characteristics
Grain boundary sliding	-	$\dot{\gamma} \propto \tau^2$; H_o equals self diffusion energy.
Diffusion creep	-	$\dot{\gamma} \propto \tau$; H_o equals self diffusion energy or grain boundary self-diffusion energy.

It is well known that the strong temperature dependence of b.c.c. metals is due to high Peierl-Nabarro stress[44,45]. Considering the movement of dislocations, the bond angles between the atoms in the core of the dislocation change and consequently the core energy changes as the dislocation moves. Such changes in the core energy are expected to be greatest for covalently bonded crystal such as Ge, Si etc. For which the bond energy changes rapidly with bond angles, and least for f.c.c. metals which have metallic binding. Coulombic interactions in ionic crystals suggest that they may exhibit intermediate changes in dislocation core energy upon motion of the dislocations.have their least[46]

Thus dislocations have their least energy when they lie in valleys parallel to close packed rows of atoms. The stress necessary to move dislocation from one valley to next valley at 0°K is the Peierl-Nabarro stress. When a dislocation is lying in a valley, the core energy is given by $E_o \simeq 0.5 \, Gb^2$ where G = shear modulus, b = Burgers vector and at the top of the hill dislocation line energy is E_m. Although several type of shapes of Peierls hill have been found through computer simulation technique based on two-atom Morse-type of potential.But for simplicity's sake the sinusoidal shape has been assumed. At

any intermediate position, the line energy will be :

$$E(y) = \frac{E_m + E_o}{2} + \frac{E_m - E_o}{2} \cos 2\bar{A} \, y/a \quad \ldots \ldots (1)$$

where a is the distance between close packed rows of atoms
on the slip plane. When part of a dislocation crosses over
the hill from one valley to next valley, it is said to be
kinked. The increase in energy of a kinked dislocation above
that of a dislocation that lies execlusively in one valley
is known as the kink energy (Un). The Un was calculated by
Dorn and Guyot[47]. It is given as

$$U_n = RT \ln \frac{P.L.a.b^2 \gamma}{2 \, w^2 \dot{\varepsilon}} \quad \ldots \ldots \ldots (2)$$

where P = dislocation density, L = dislocation length,
a = mean distance between valleys, b = Burgers vector,
w = width of the kink separation, • = strain rate,
T = absolute temperature, R = Universal gas constant, and
γ = Debye frequency. Actually during the motion of a dislo-
cation from one valley to the next one, there are two steps.
The first one is the nucleation of pair of kinks and the
second one is the separation of the kinks. It is considered
that the formation of a double kink is the more difficult
process than their separation. Thus double kink nucleation
is the rate controlling process.

The interesting feature of the equation (2) is that
Un varies linearly with temperature. As it is mentioned in
the table that V^* will not vary with strain since in Peierls
mechanism the linear obstacles controls the dislocation move-

ment . So whatever be the density of dislocations, it will not in any way alter the nature of the linear obstacles, since it is the inherent lattice characteristic of the material.

In our investigations, we have found[i] a strong temperature dependence of flow stress (fig.25). (ii) V^* does not change with strain (fig.(28))(iii) H varies linearly with temperature, Fig.(29).

Thus it can be inferred that Peierls-Nabarro mechanism is the rate controlling process in the plastic deformation of $CuAl_2$ intermetallic.

Moreover, with similar approach, the same mechanism has been established in other systems e.g. B.c.c. metals at cryogenic temperatures, H.c.p. metals, alloys, intermetallics in non-basal slip, B2 alluminide (NiAl), Ll_2 intermetallics Cu_3Au (14), Pt_3Al (49) and ionic solid NaCl (50), CaF_2(48) etc.

The H and V^* values associated with the plastic deformation of $MgZn_2$ (13) are 2 eV and $27b^3$ respectively and that the deformation has been explained in terms of Peierls-Nabarro mechanism. Moreover, the previous observation on $CuAl_2$ by Dey and Tyson (15) compares favourably with the results of this study. The large H and small V^* values are undoubtedly due to complexity of crystal structure and probably due to directional nature of bonding. All these evidences conclusively prove that the rate controlling mechanism is the Peierls-Nabarro type. One

of the most striking observations in our $CuAl_2$ intermetallics is the applicability of Peierls mechanism upto 575°C (0.98Tm).

If the flow stress of single crystal and polycrystal is compared at a given temperature, it may be noted that there is a grain size strengthening effect in addition to the lattice frictional stress. Thus the flow stress of a polycrystalline specimen at a given temperature can be considered as the sum of lattice frictional stress and grain size contribution. From the nature of observed flow stress variation in polycrystalline specimens with temperature, it appears that the grain size strengthening effect is essentially in the form of change in athermal component of flow stress. Further, the grain size strengthening is found to be represented by Hall-Petch relation. What is surprising in this regard is that the Hall-Petch relation is valid upto .98 Tm. This is contrary to the usual observations on metals in which grain size weakening effect occurs above 0.5 Tm in general. This strength retention of the grain boundaries at high temperatures may possibly be arising from the nature of grain boundaries and their structure in $CuAl_2$. Thus while the dominance of Peierls mechanism continues upto 0.98 Tm specially for P/m sample, the grain size strengthening is also retained simultaneously.

However, while the P/m sample has almost the same stress exponent both at 475°C and 575°C, the different stress exponent values of the single crystal suggest a change of

mechanism at temperatures close to the melting point. In view of the high activation energy for flow compared to the inter-diffusional activation energy identification of the very high temperature flow mechanism in single crystals is, however, not possible on the basis of present observations.

Further it may also be noted that the interdiffusional activation energy (1.32 eV) of $CuAl_2$[50] is significantly smaller than the activation energy for deformation (e.g. 4 eV at 525°C). Thus diffusion does not seem to be important in the context of operative deformation mechanism even at temperatures close to the melting point (0.98 Tm) of $Cu Al_2$.

CHAPTER V

CONCLUSIONS

(1) The brittle-ductile transition temperature of both single crystal and polycrystalline $CuAl_2$ specimens prepared through P/m route is around .75 Tm and for as cast sample, it is around .77 Tm (Tm = melting point).
Thus, the B.D.T. temperature is not sensitive to grain size variation.

(2) Introduction of mobile dislocations by a small prestrain has resulted in a lowering of B.D.T. temperature.

(3) Considerable strengthening is achieved through grain refinement over the temperature range 425°C to 575°C.

(4) The Hall-Petch relation is found to be valid over the whole temperature range upto 0.98 Tm.

(5) The flow stress is very sensitive to temperature like b.c.c. metals.

(6) The rate controlling mechanism for deformation is the Peierls-Nabarro lattice frictional stress.

(7) The activation energy for flow is considerably higher than that for diffusion even at 575°C (0.98 Tm) and activation volume is below $20b^3$.

REFERENCES

(1)   J.H.Westbrook : Intermetallic Compound : their past Promise., Met. Trans. Vol. 8A. No.9, Sept.1977, Page 1327-1360.

(2)   R.E.Smallman : Modern Physical Metallurgy - Butterworth Co.London, 1962.

(3)   W.Hume-Rothery and G.V.Raynor : The Structure of Metals and Alloys Inst. of Metals, Monograph and Report Series- London, 1954.

(4)   C.S.Barrett, T.B.Massalski: Structure of Metals - 3rd Ed. McGraw Hill, N.Y.1966.

(5)   N.S.Stoloff : Intermetallic compounds and ordered phases in Strengthening methods in Crystal - Ed. by A.Kelly and R.B.Nicholson, Applied Science Publishers Ltd.,London, 1971.

(6)   M.J.Marcinkowski - Phys. Stat. Sol(a) 90, 621 (1985).

(7)   E.M.Schulson et al - Scripta-Metall. 19(1985), p.1497.

(8)   L.Von Mises. 1928, Z. Angew Math. Mech. 8, 161.

(9)   A.Ball and R.E.Smallman, 1966, Acta. Metall., 14, 1349.

(10) E.M.Schulson and D.R.Barkar - Scripta-Met. 17 (1983), p. 519.

(11) M.J.Marcinkowski and N.Brown. 1961, Acta. Met. 9, 764.

(12) N.S.Stoloff and R.G. Davies,1964, Trans. A.S.M.57, 247.

(13) P.Paufler and G.E.R.Schulze, Phys. Stat. Sol.24, 77 (1967).

(14) A.G.Evans and R.D.Rawlings., Phys. Stat. Sol. 34, 9 (1969).

(15) B.N.Dey and W.R.Tyson, Phys. Stat. Sol.(a) 9, 215 (1972).

(16) J.H.Westbrook and D.L.Wood, T.of Inst.Of Metals 1962-63, Vol. 91, p. 174.

(17) N.S.Stoloff and R.G.Davies: Prog. Mat. Sci. 13(1966) 3-84.

(18) E.M.Schulson, Symp. High Temp. Ordered Intermetallic Alloys (Mrs. Symp. Proc. Vol.39)., Pittsburgh (1985).

(19) E.M.Schulson et al. Acta Metall. 33 (1985) 1587-1591.

(20) I.Baker and P.R.Munroe : J.of Metals Feb. 1988, p. 28

(21) H.A.Lipsitt: Symp. High-Temperature Ordered Intermetallic alloys (Mrs. Symp. Proc. Vol.39) C.C.Koch, C.T.Liu and NS Stoloff (eds), Mat. Res.Soc., Pittsburgh (1985) p.351-364.

(22) E.M.Schulson, Int. Met. Rev. 29 (1984) 195-209.

(23) J.A.Horton and C.T.Liu, Acta Metall. 33 (1985) 2191-2198.

(24) V.Vitek and D.P.Pope, in Ref. 21, p. 205-212.

(25) C.T.Liu et al in Proc. Symp. High Temp. Materials Chemistry II ed. Munir et al (The electrochemical Society, 1983).

(26) C.T.Liu and H.Inouye - Metal. Trans.A, 10A (1979) p.1515.

(27)   J.Sehiliting, High Temp. High Pressures 10 (1978) 241-269.

(28)   M.Ignat and F.Durand - Phys. Stat. Sol.(a) 51, 567 (1979).

(29)   J.J.Gniewek and C.A.Wasik. J.Appl. Phys. 'Communication' 1970.

(30)   H.Zogg. J.Appl.Cryst. (1979), 12, 91-94.

(31)   E.E.Havinga et al. J.Less Common Metals. 27 (1972) p.179.

(32)   W.B.Pearson, Handbook of Lattice Spacings and Structures
       of Metals and Alloys, Vol.I, and II. Pergamon Press,
       Oxford, 1958 and 1967.

(33)   G.Hägg, Phys. Z. Phys. Chem. 1312 (1931) 413.

(34)   Haansen and Anderko - Constitution of Binary Alloys -
       Ed.58, McGraw Hill.

(35)   F.R.Eshelman (1975), Ph.D. Thesis, Iowa State University.

(36)   J.Karou and N.V.Youdelis - Communication, Mat.Sci. and
       Tech. May (1987) Vol.3.

(37)   P.N.F. Blane. et al - Appl. Cryst. (1979). 12. 151-155.

(38)   R.Cabarat et al - (1948), C.R. Aca. Sci. 226, 1374-1376.

(39)   R.Kirsten - Montsbar. Dtsh. Akad. Wiss, Berlin 4, 496, 1962.

(40)   M.Ignat and F.Durand - Scripta-Met. Vol.10, p. 623-626, 1976.

(41)   E.R.Petty, J.Inst. Of Metals 60-61, Vol. 89.

(42)   R.Schmidt - Whitley - Z.Metall Kunde, 61, 552, (1973).

(43)   E.A.Little. The J.Of Aust. Inst. of Metals -Vol. 21, No.1
       March 1976.

(44)   H.Conrad,'The Cryogenic Properties of Metals' in High-
       Strength Materials, Proc. of the second Berkeley International
       Materials Conf. June 15-18, 1964, Ed.By Victor F.Zackay.

(45) G.S.Murty, J. of Materials Sci. 21 (1986) 211-216.

(46) J.E. Dorn and S.Rajnak . Trans. A.I.M.E. Vol. 230, 1964, p.983

(47) J.E.Dorn and P.Guyot. Canad. J.of Physics, Vol.45, 1967.

(48) G.Tichy, V.Vitek and D.P.Pope - Symp.

(49) A.Arieli, H.C. Heard, and A.K.Mukherjee on Deformation
       modelling in Sodium Chloride - in Mechanical testing for
       deformation model development ed. by Rhode and Swearengen.
       A.S.T.M. STP 765, Symp. on Mech.Testing A.S.T.M.12-13 No.V 198(

(50) Y.Funamizu and K.Watanbe. Trans. JIM 1971, Vol.12, p.147-152.

(51) J.D.Whittenberger - Mat.Sci. and Engg., 77 (1986) 103-113.